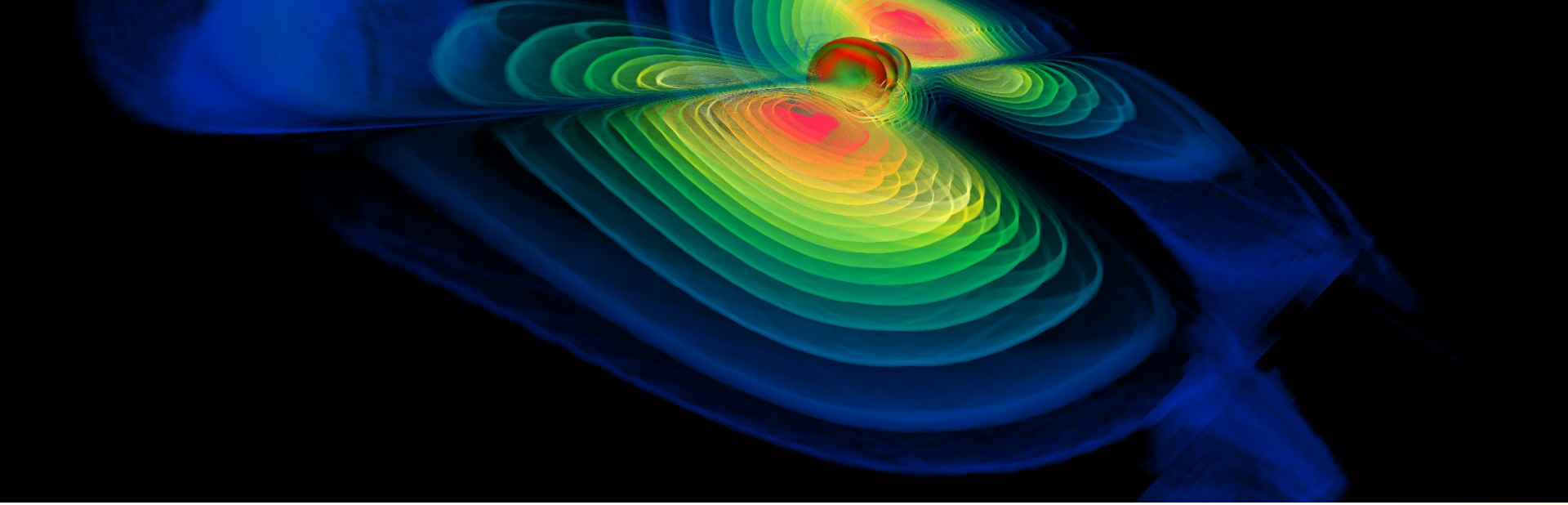

Precessing black hole binaries and their gravitational radiation

László Árpád GERGELY

Institute of Physics, University of Szeged

With

Márton Tápai, Zoltán Keresztes

10th Bolyai-Gauss-Lobachevsky Conference, **2017**, Eszterházy Károly University, Gyöngyös, Hungary

General relativity, the theory of gravitation

1. Matter tells space-time how to curve (Einstein equation)

$$R_{\mu\nu} - \frac{1}{2} R\, g_{\mu\nu} + \Lambda\, g_{\mu\nu} = \frac{8\pi G}{c^4} T_{\mu\nu}$$

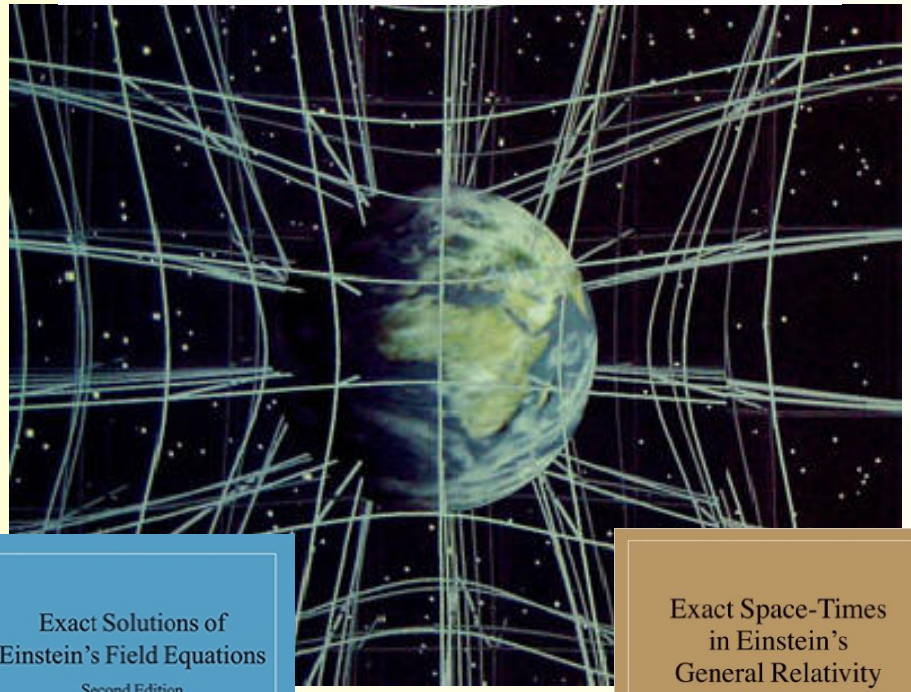

2. Space-time tells matter, how to move (geodetic equation)

$$\frac{d^2 x^\mu}{ds^2} = -\Gamma^\mu{}_{\alpha\beta} \frac{dx^\alpha}{ds} \frac{dx^\beta}{ds}$$

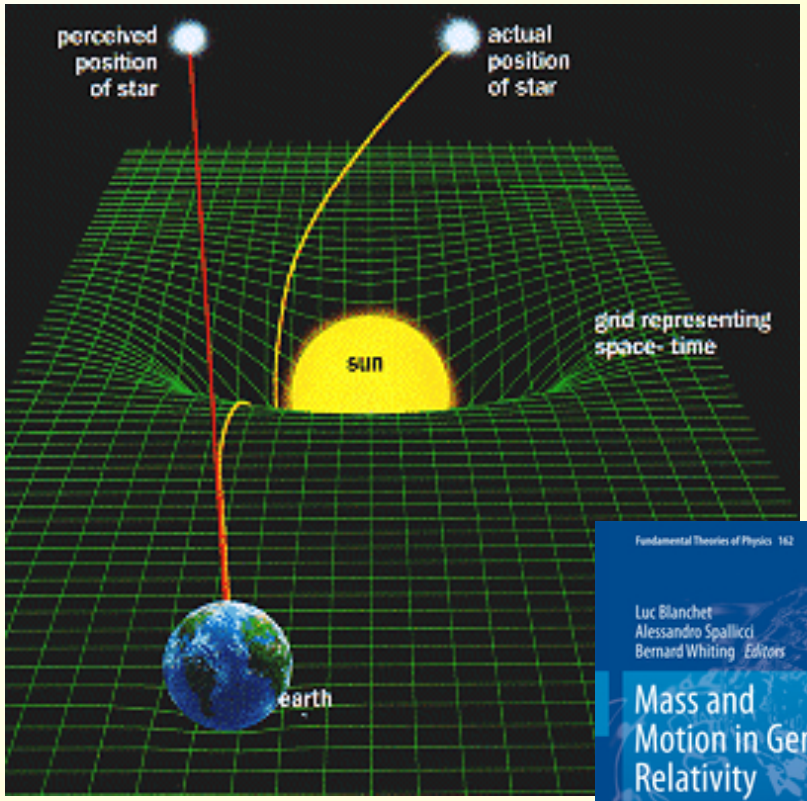

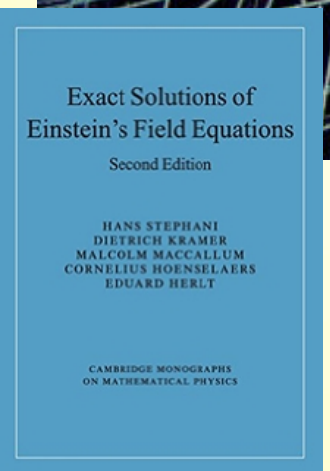

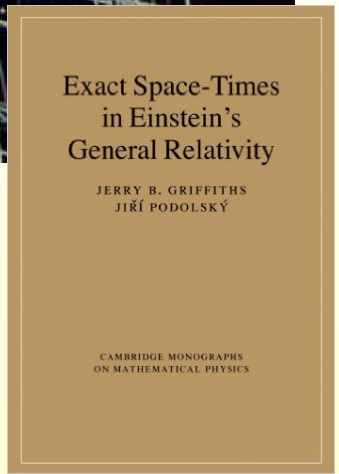

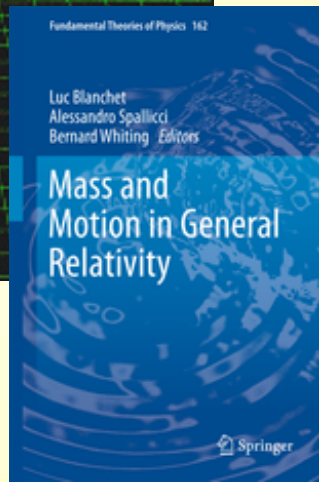

New effects, concepts

New (weak-field) effects in the Solar System:

- perihelion precession of Mercury
- gravitational light deflection (Solar Eclipse)
- gravitational redshift / time dilation (GPS)
- Shapiro-delay / radar echo delay

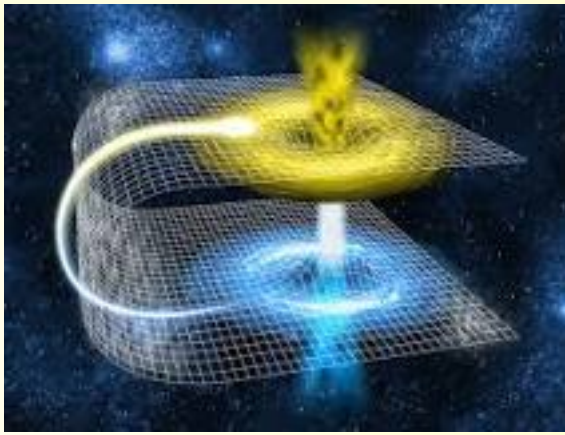

New concepts:

- black hole

from stellar evolution $M \leq 20M_\odot$

intermediate mass $20M_\odot < M < 10^5 M_\odot$

supermassive

- wormhole

EP=EPR, relation to quantum field theories?

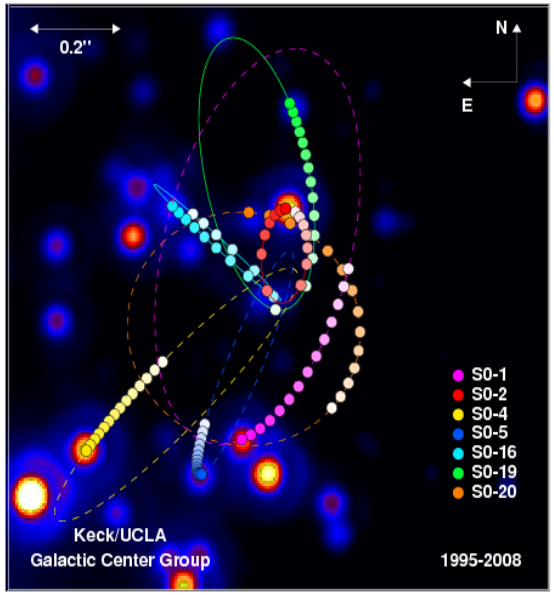

- gravitational (micro)lensing

LHC has not seen supersymmetry

→ dark matter is not WIMP

MACHO observations (Large Magellanic cloud)

→ at most 10% of dark matter from stellar evolution

→ intermediate mass, primordial black holes account for dark matter?

(need for a dedicated observation program)

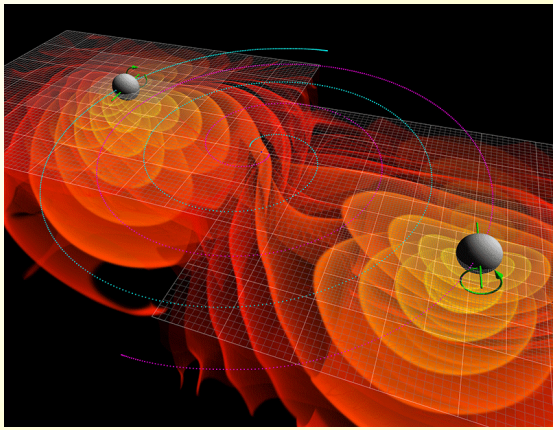

- gravitational radiation

How do we see black holes?

John Archibald Wheeler:

From the movie on gravitational waves, in preparation,
by Boglárka H. Molnár

Stars orbiting the supermassive black hole in the center of the Milky Way

large curvature → black hole

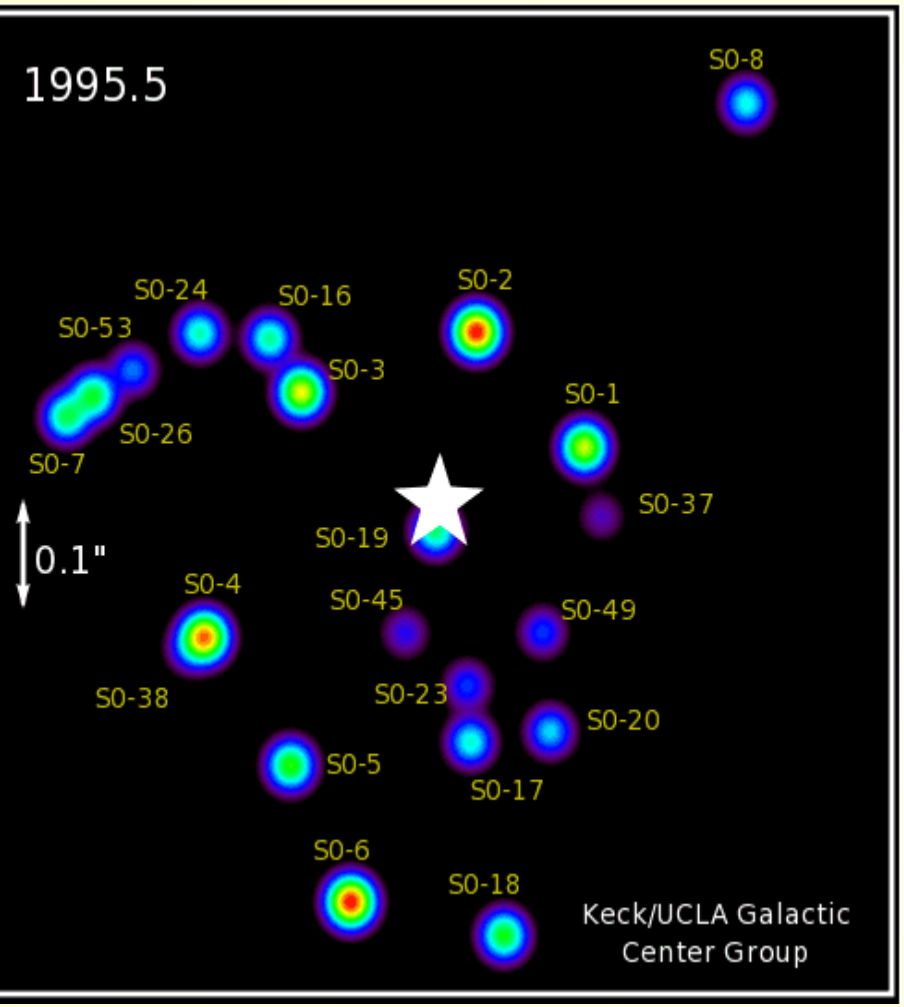

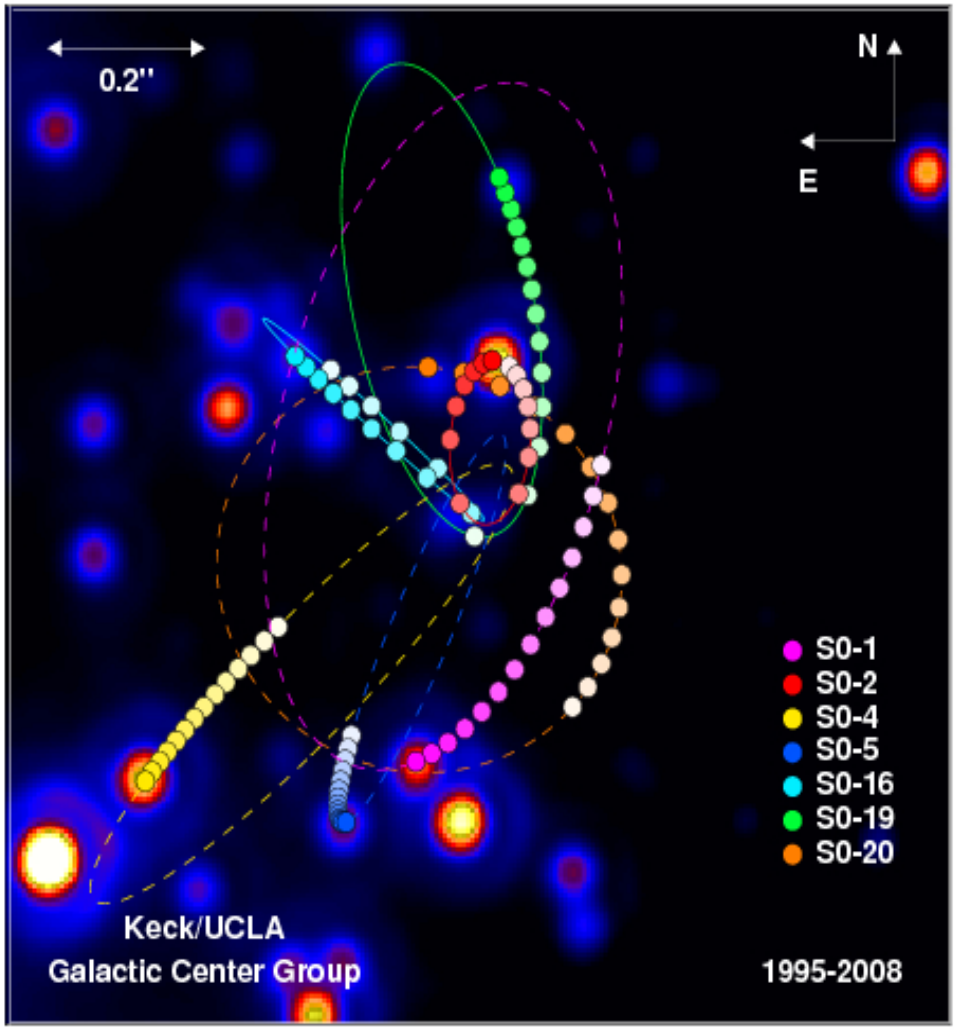

Accretion by black holes with disk and jet

Maximal spin and energy conversion efficiency in a symbiotic system of black hole, disc and jet
Z. Kovács, L. Á. Gergely, P. L. Biermann, Mon. Not. R. Astron. Soc. **416,** 991–1009 (2011)

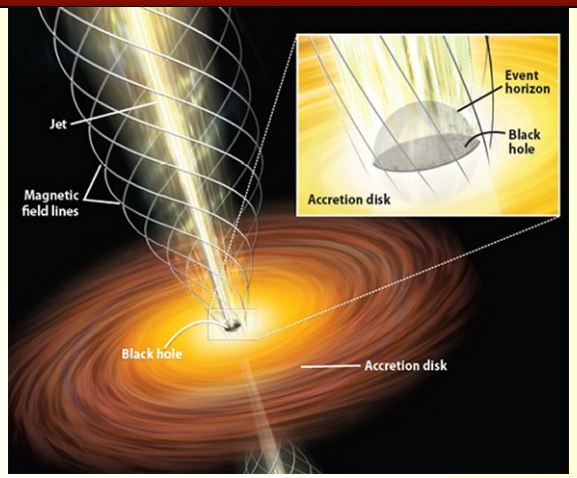

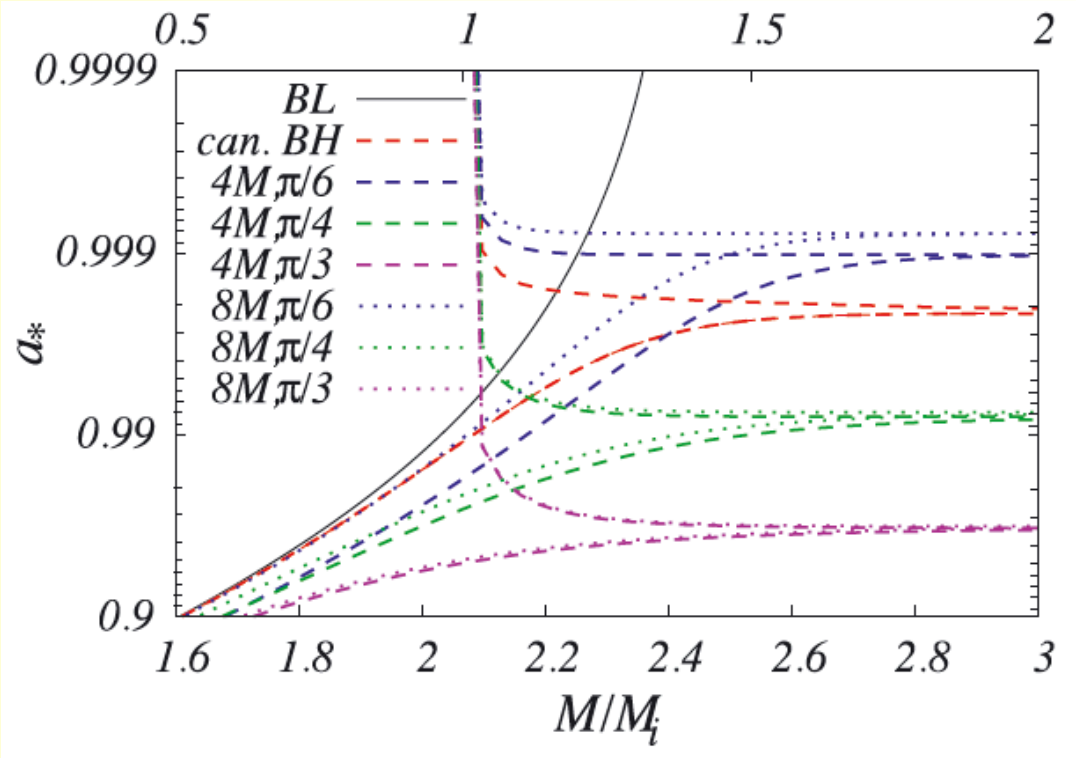

θ_{max}	n	a_* (I)	ϵ (I)
$\pi/6$	1	0.8961	0.309
	2	0.8901	0.301
	3	0.8803	0.285
$\pi/4$	1	0.8976	0.312
	2	0.8933	0.306
	3	0.8872	0.298
$\pi/3$	1	0.8969	0.310
	2	0.8948	0.308
	3	0.8924	0.305
$\pi/6$	1	0.8968	0.311
	2	0.8901	0.302
	3	0.8822	0.291
$\pi/4$	1	0.8983	0.313
	2	0.8939	0.308
	3	0.8879	0.300
$\pi/3$	1	0.8975	0.312
	2	0.8955	0.311
	3	0.8931	0.307

Gravitational lensing by a black hole

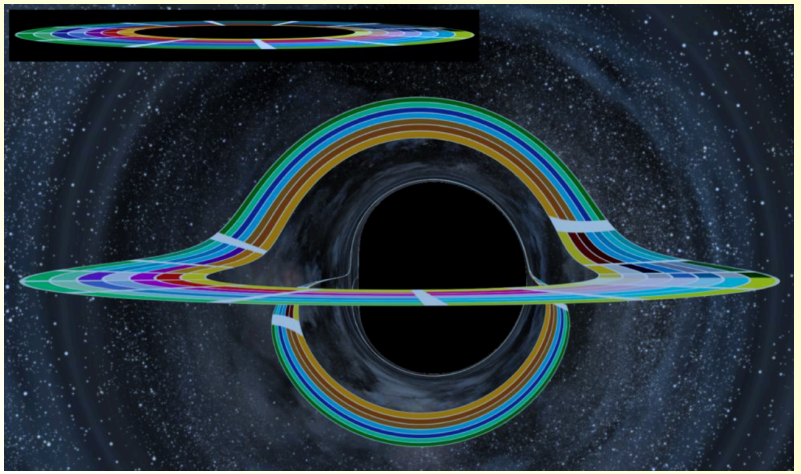

The black hole:

- Deflects the light from the accretion disk
- Provides two images of it

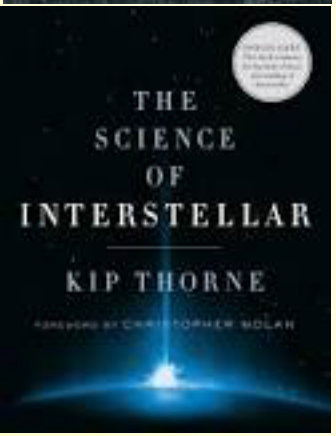

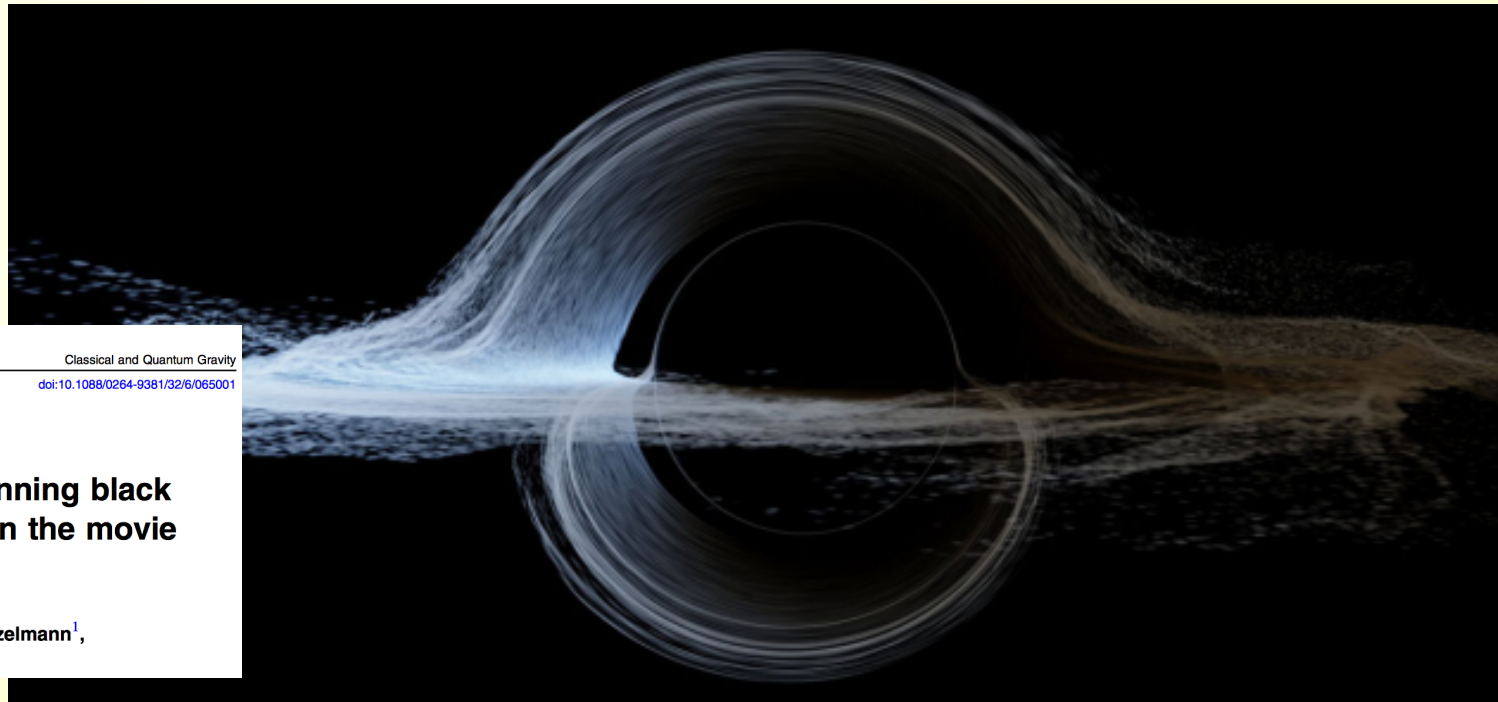

OPEN ACCESS
IOP Publishing
Classical and Quantum Gravity
Class. Quantum Grav. **32** (2015) 065001 (41pp)
doi:10.1088/0264-9381/32/6/065001

Gravitational lensing by spinning black holes in astrophysics, and in the movie *Interstellar*

Oliver James[1,*], Eugénie von Tunzelmann[1], Paul Franklin[1] and Kip S Thorne[2]

Gravitational lensing by a coalescing black hole binary

Electromagnetic signatures of coalescing black hole binaries in jets

See next talk by Emma Kun

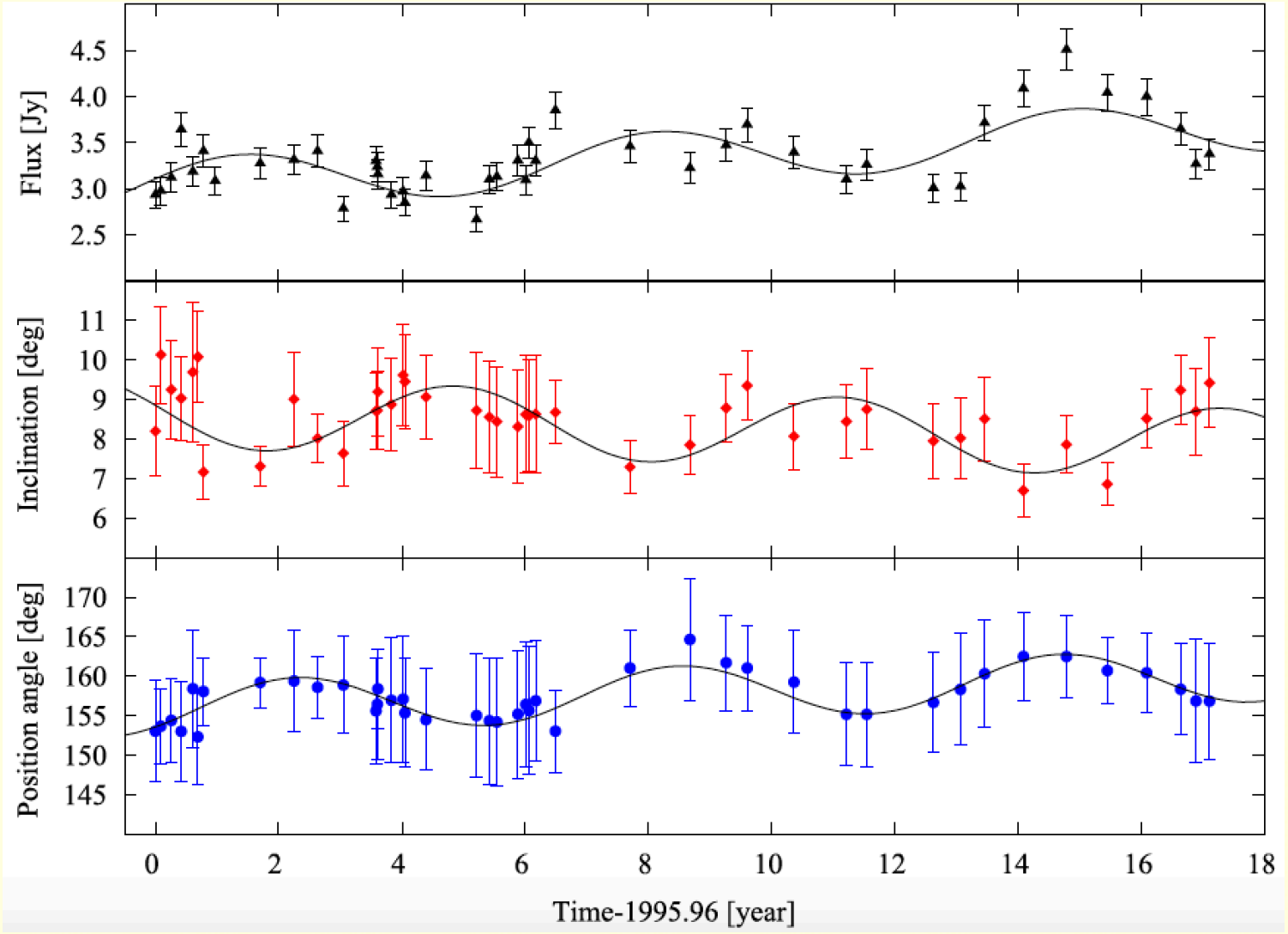

A spinning supermassive black hole binary model consistent with VLBI observations of the S5 1928+738 jet
E. Kun, K. É . Gabányi, M. Karouzos, S. Britzen, L. Á. Gergely, MNRAS **445,** 1370–1382 (2014)

High-energy neutrinos from the aftermath of black hole binary coalescence

The neutrino emission is due to energetic proton–proton collisions, where the kinetic energy of the protons is above the energy threshold of pion-creation.

See next talk by Emma Kun

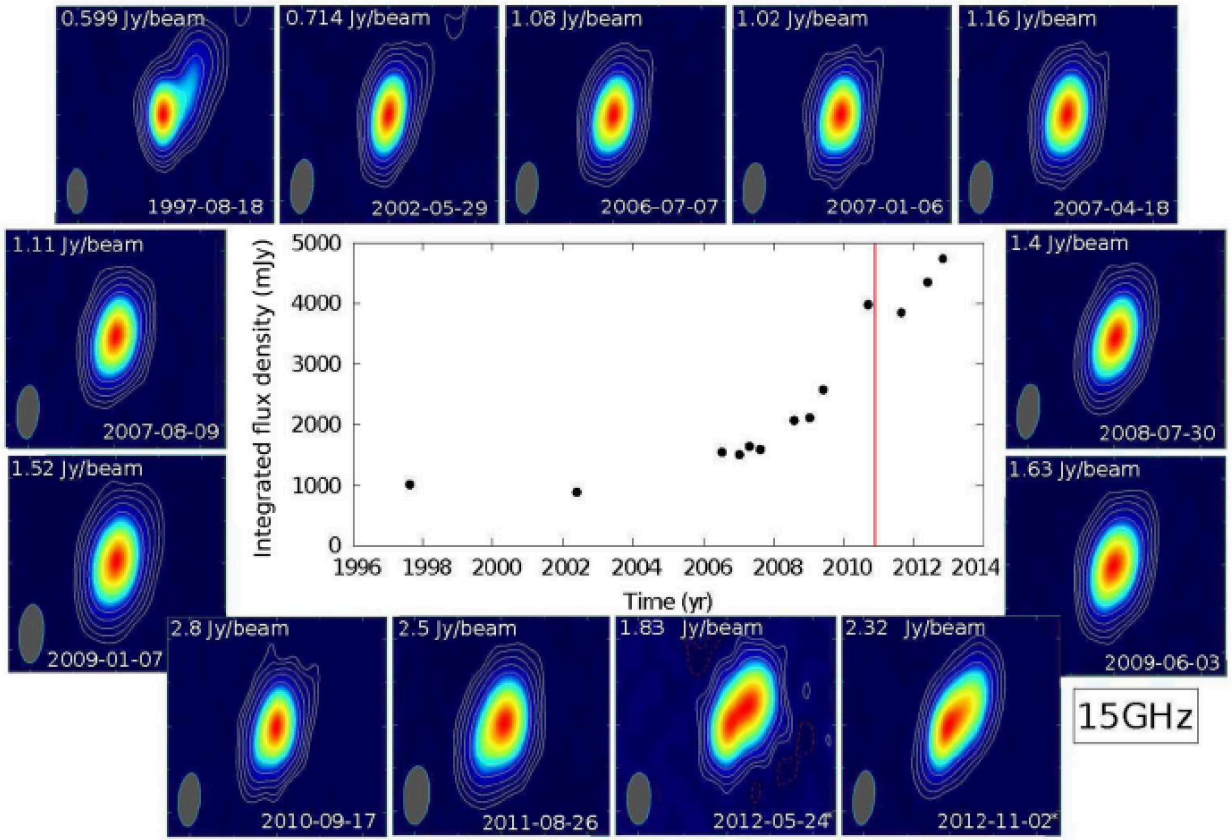

Figure 2. The radio maps of PKS 0723−008 over 12 epochs, represented on logarithmic scale with base 10. They were produced by processing the available VLBA visibilities provided by the MOJAVE team. Iso-flux density contours are in per cent of the peak flux density marked in the left upper corner of the maps. They increase by factors of 1, except the last two epochs (marked by stars), where the contours increase by factors of 2. In the middle, the integrated flux density of the source at 15 GHz is represented as a function of the time. The time of the corresponding neutrino detection (ID5) is indicated by a red vertical line.

A flat-spectrum candidate for a track-type high-energy neutrino emission event, the case of blazar PKS 0723−008
E. Kun, P. L. Biermann, L. Á. Gergely, MNRAS **466,** L34–L38 (2017)

Gravitational radiation from a coalescing black hole binary

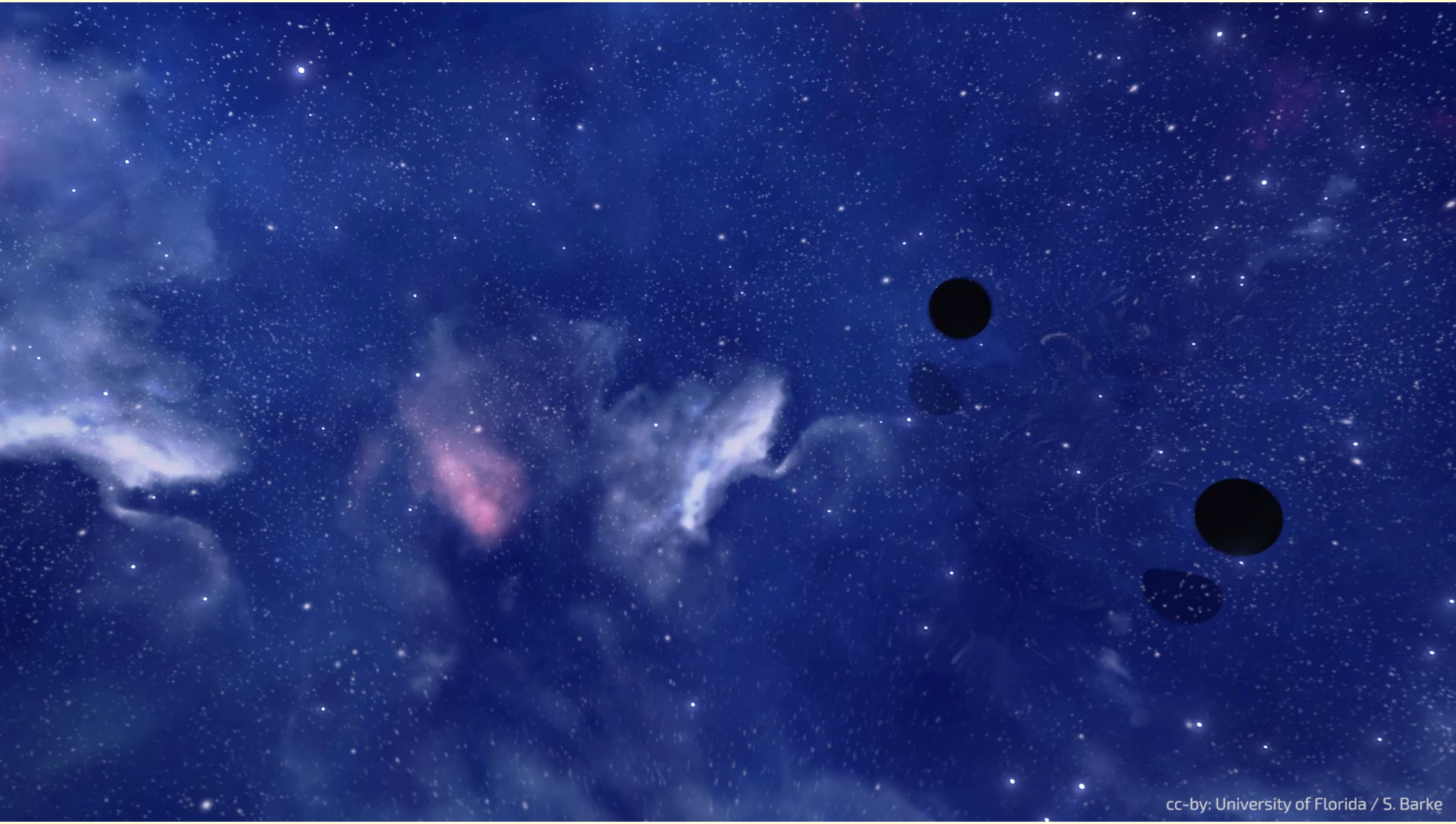

What happens when this gravitational radiation reaches the Earth?

Luckily there are no close coalescing black hole binary systems!!

The network of second generation interferometric gravitational wave detectors

Advanced LIGO, Hanford, USA, 4km

Advanced LIGO, Livingston, USA, 4km

Advanced Virgo, Cascina, Italy, 3km

KAGRA, Kamioke, Japan, 3km

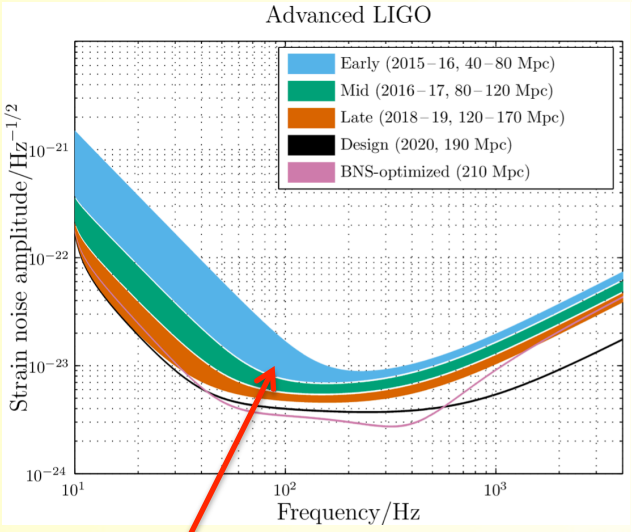

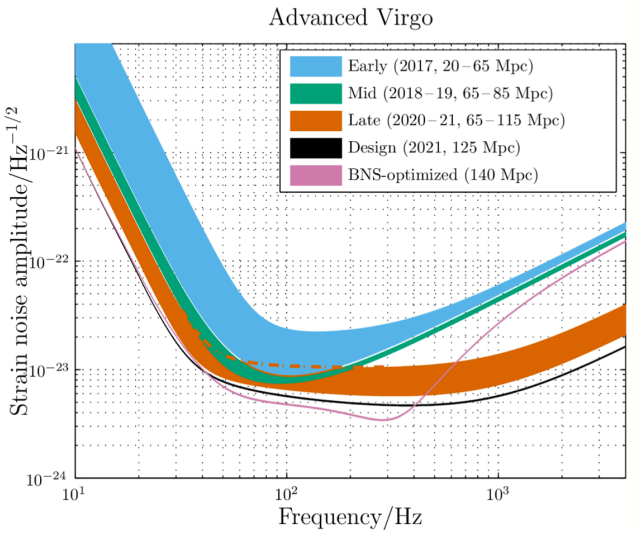

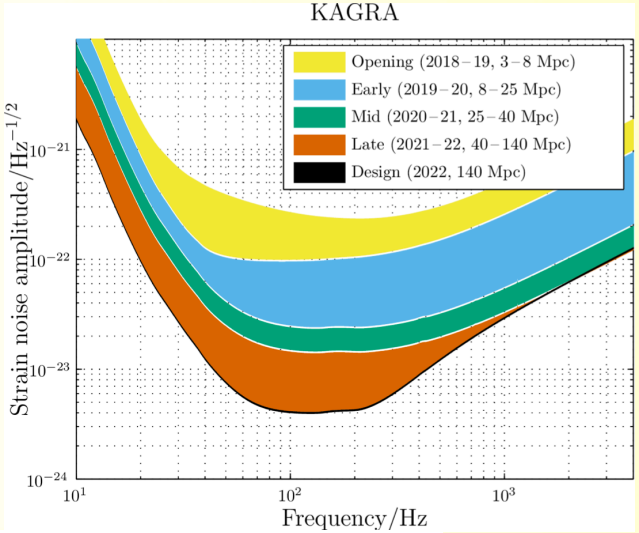

GW150914
GW151226
GW170104

Table 1 Plausible target detector sensitivities. The different phases match those in Figure 1. We quote the range, the average distance to which a signal could be detected, for a $1.4M_\odot$+$1.4M_\odot$ binary neutron star (BNS) system and a $30M_\odot$+$30M_\odot$ binary black hole (BBH) system.

	LIGO		Virgo		KAGRA	
	BNS range/Mpc	BBH range/Mpc	BNS range/Mpc	BBH range/Mpc	BNS range/Mpc	BBH range/Mpc
Early	40 – 80	415 – 775	20 – 65	220 – 615	8 – 25	80 – 250
Mid	80 – 120	775 – 1110	65 – 85	615 – 790	25 – 40	250 – 405
Late	120 – 170	1110 – 1490	65 – 115	610 – 1030	40 – 140	405 – 1270
Design	190	1640	125	1130	140	1270

First direct detection of gravitational waves: GW150914

Phys. Rev. Lett. **116**, 061102 (2016)

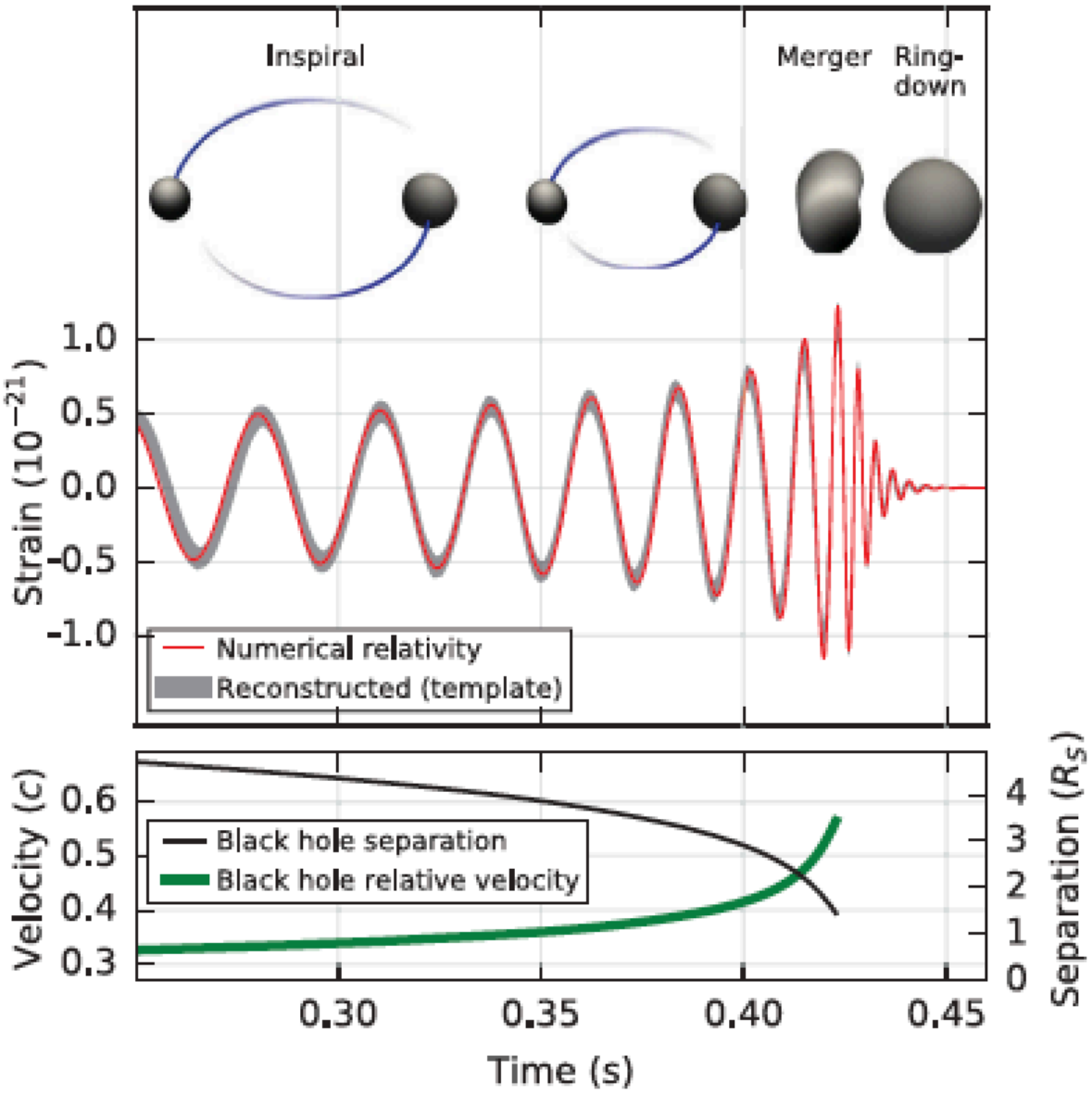

Coalescence of black holes of 29 and 36 solar masses → over 05 sec the energy equivalent of 3 solar masses was emitted in the form of gravitational waves = The energy production of the Paks Nuclear Plant over 10^{31} years !

Due to the large distance Advanced LIGO registered one part in a thousant change of the proton size !

This event occurred 1.3 billion years earlier , when the oxygen filled atmosphere was formed on the Earth !

Where was GW150914 coming from? (230-500 Mpc)

Milky Way ~ 30 kpc

Laniakea supercluster ~ 160 Mpc

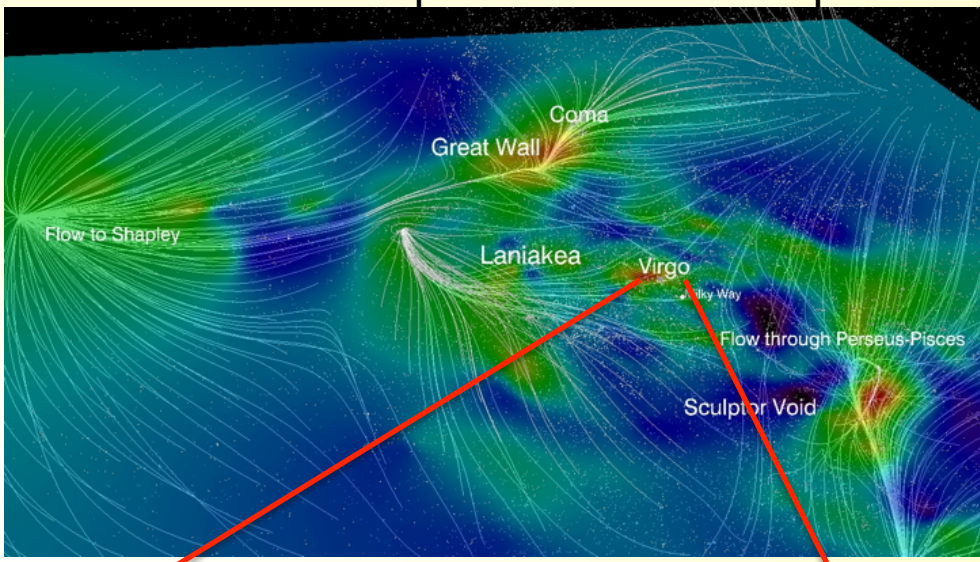

Local Group ~ 3,1 Mpc

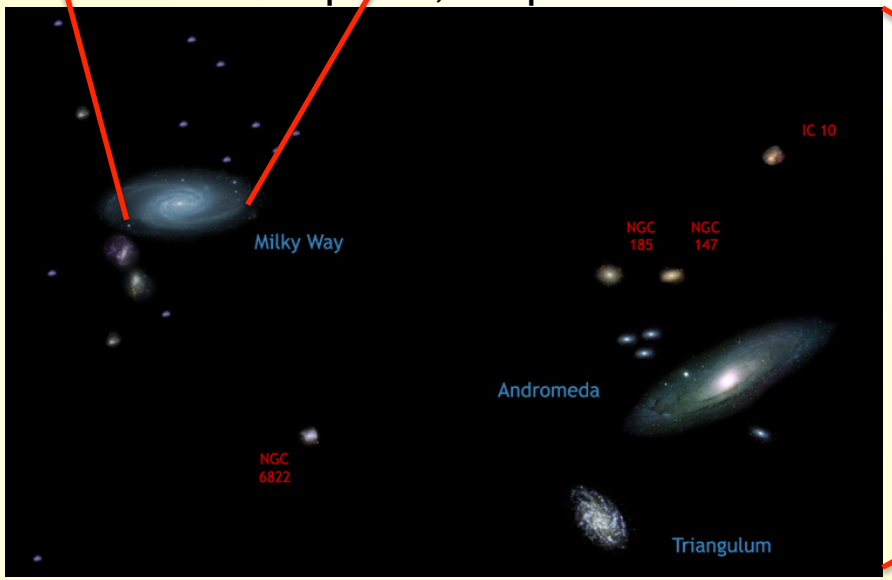

Virgo supergroup ~ 33 Mpc

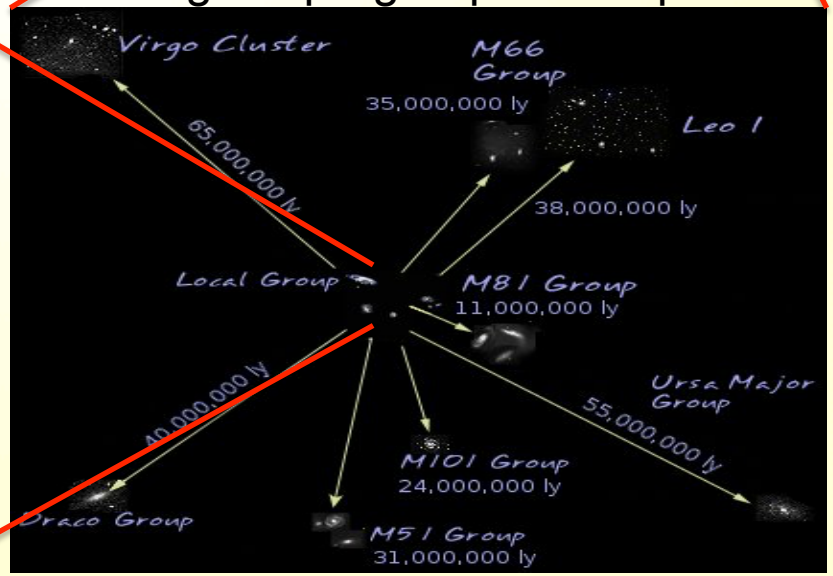

Opens up a new way to map the local Universe

https://pionic.org/motions-of-thousands-of-galaxies-mapped
https://player.vimeo.com/video/206210825?byline=0&badge=0&portrait=0&title=0&api=1&autoplay=1

Motions Of Thousands Of Galaxies Mapped

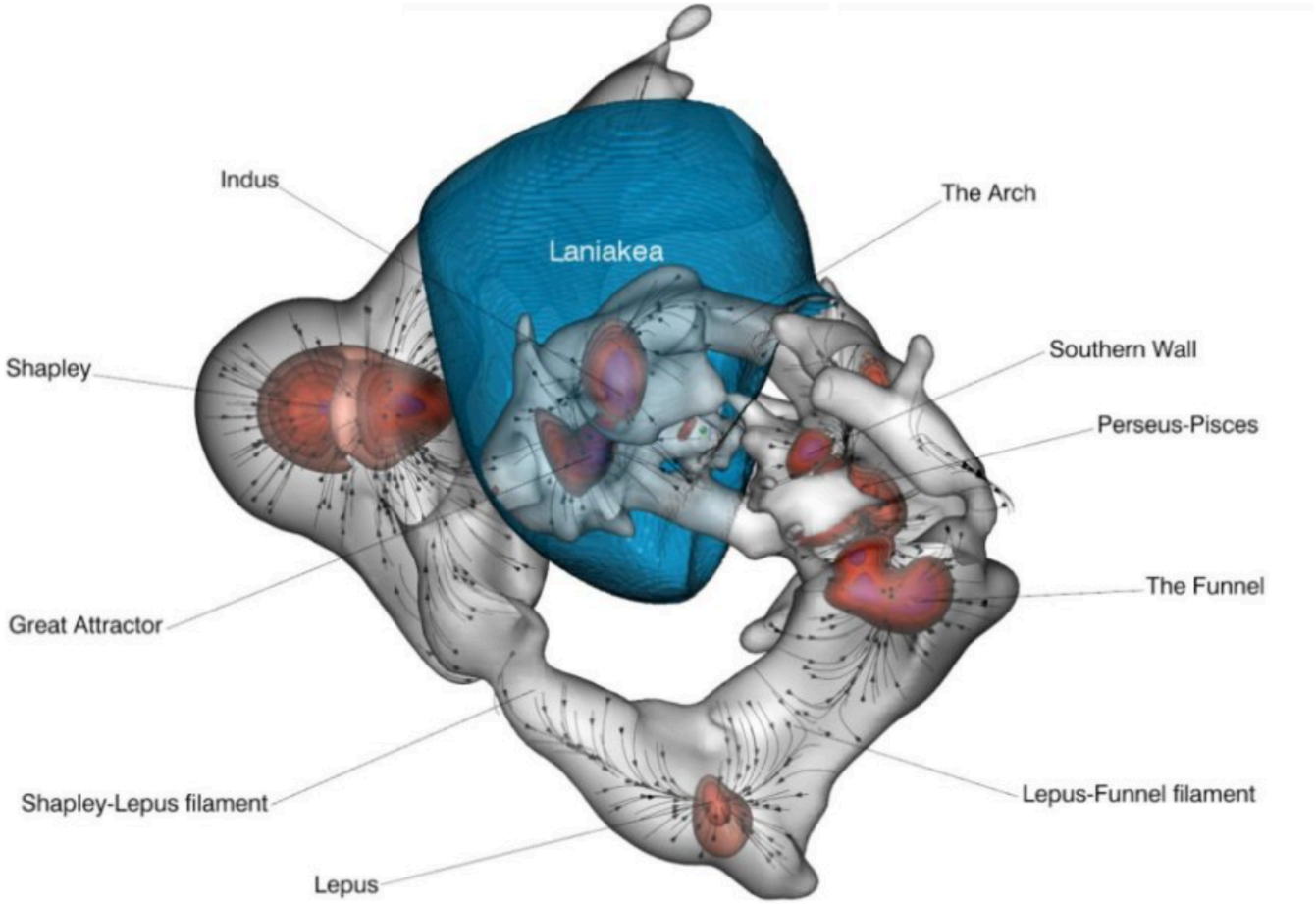

The cosmic velocity web is represented by surfaces of knots in red and surfaces of filaments in gray. The black lines with arrows illustrate local velocity flows within filaments and toward knots. The Laniakea Supercluster basin of attraction that includes our Milky Way galaxy is represented by a blue surface. The region being displayed extends across one billion light years. Credit: Daniel Pomarede, Yehuda Hoffman, R. Brent Tully and Helene Courtois. Credit: Daniel Pomarede, Yehuda Hoffman, R. Brent Tully, Helene Courtois

Black hole binary systems in a post-Newtonian (PN) approach

Non-spinning gravitational waveform

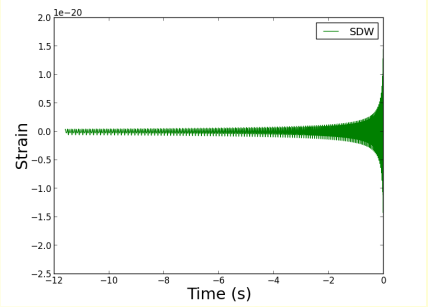

Spinning gravitational waveform

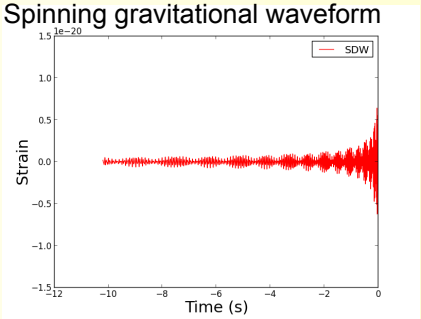

Validity:

- far from the horizon
- at small velocities compared to the speed of light

Perturbed Kepler dynamics:

- corrections from general relativity 1PN, 2PN, ...
  (modify the shape of the orbit)
- spin corrections 1.5 PN, 2PN, ...
  (modify the orbital plane)
- gravitational radiation 2.5 PN, ...
  (take out energy, momentum, angular momemtum from the system)

In general relativity
gravitational radiation
emerges in two polarisations:
(as their linear combination)

In scalar-tensor gravity theories there are 4 additional polarisations!
(see this afternoon talks by
Cecília Nagy and Bence Racskó)

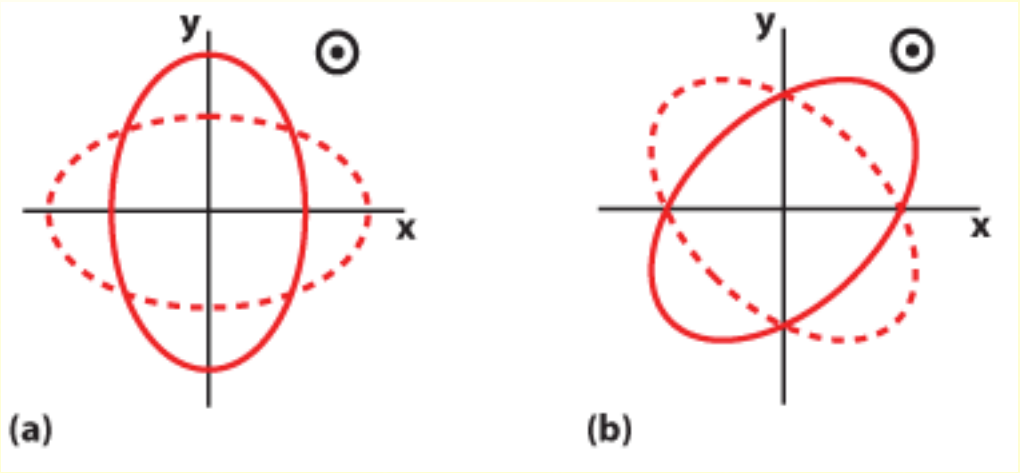

Black hole binary systems: the 2PN conservative dynamics

Binary and spin dynamics to 2PN accuracy, including leading order spin-orbit, spin-spin and mass quadrupole-mass monopole effects, for generic (noncircular, nonspherical) orbits

Involved, but closed system of first order ordinary differential equations for osculating orbital elements and spin angles

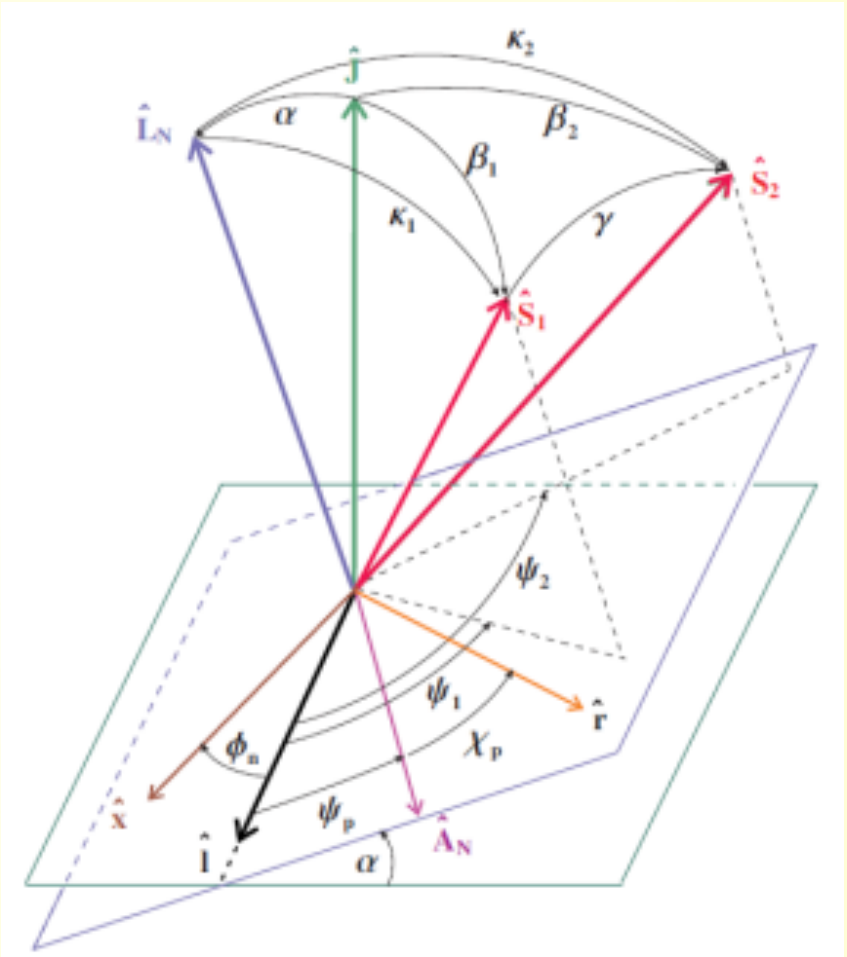

Spinning compact binary inspiral: Independent variables and dynamically preserved spin configurations
L. Á. Gergely, Phys. Rev. D **81**, 084025 (2010)

Spinning compact binary inspiral. II. Conservative angular dynamics
L. Á. Gergely, Phys. Rev. D **82**, 104031 (2010)

Application 1: the chameleon orbits (equal masses)

We show the existence of chameleon orbits, whose local, orbital parameters evolve from elliptic (in the Newtonian sense) near pericenter, towards hyperbolic at large distances

Behavior consistent with the picture that general relativity predicts stronger gravity at short distances than Newtonian theory does

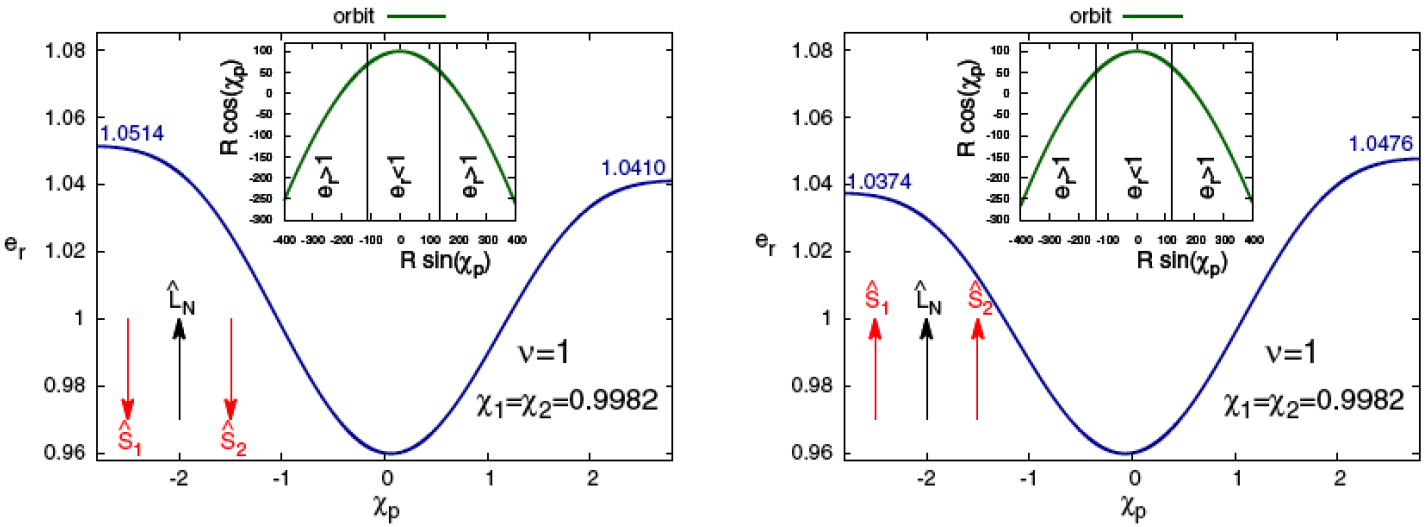

FIG. 2 (color online). Chameleon orbits due to 1PN and SO effects for binaries with equal masses and spins ($\chi_1 = \chi_2 = 0.9982$). The curves and initial conditions are as on Fig. 1. On the left (right) panel the spins are antialigned (aligned) with the orbital angular momentum.

Spinning compact binary dynamics and chameleon orbits
L. Á. Gergely and Z. Keresztes, Phys. Rev. D **91**, 024012 (2015)

Application 1: the chameleon orbits (mass ratio 1:30)

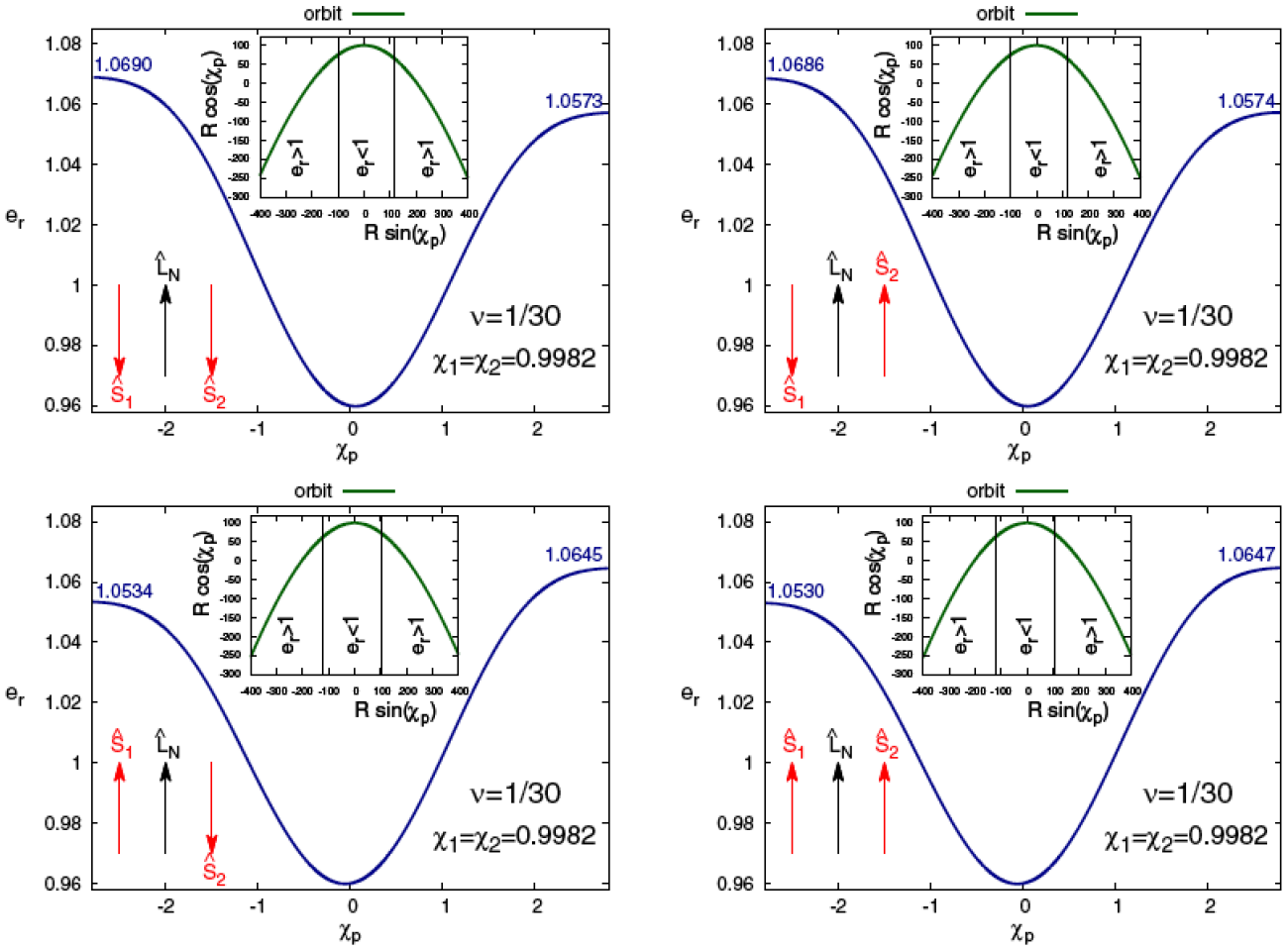

FIG. 3 (color online). Chameleon orbits created by 1PN and SO effects are represented for unequal mass ($\nu = 1/30$) spinning binaries. The same functions as on Fig. 1 are shown for the same initial conditions. The relative direction of the spins and the orbital momentum are indicated by arrows. The dimensionless spin values are the same $\chi_1 = \chi_2 = 0.9982$ in all panels.

Spinning compact binary dynamics and chameleon orbits
L. Á. Gergely and Z. Keresztes, Phys. Rev. D **91**, 024012 (2015)

The 2PN secular dynamics

Secular precessing compact binary dynamics, spin and orbital angular momentum flip-flops
M.Tápai, Z. Keresztes, L. Á. Gergely, LIGO Document P1600207, submitted to Phys. Rev D

- conservative secular evolution of precessing compact binaries to 2PN order accuracy, with leading-order spin-orbit, spin-spin and mass quadrupole-monopole contributions included
- closed system of first-order ordinary differential equations evolves the pairs of polar and azimuthal angles of the spin and orbital angular momentum vectors together with the periastron angle
- In contrast with the instantaneous dynamics, the secular dynamics is autonomous

Shape parameters (equivalent to semilatus rectum and eccentricity) stay constant:

$$\bar{\dot{l}}_r = \bar{\dot{l}}_r^{PN} = \bar{\dot{l}}_r^{SO} = \bar{\dot{l}}_r^{SS} = \bar{\dot{l}}_r^{QM} = \bar{\dot{l}}_r^{2PN} = 0$$

$$\bar{\dot{e}}_r = \bar{\dot{e}}_r^{PN} = \bar{\dot{e}}_r^{SO} = \bar{\dot{e}}_r^{SS} = \bar{\dot{e}}_r^{QM} = \bar{\dot{e}}_r^{2PN} = 0$$

→ The 2PN secular dynamics is simpler then the instantaneous dynamics

The 2PN secular dynamics: Euler angles

Inclination:

$$\bar{\dot{\alpha}}^{PN} = 0 \ ,$$

$$\bar{\dot{\alpha}}^{SO} = \frac{\eta\pi}{\mathfrak{T}\,\bar{\mathfrak{l}}_r^3}\sum_{k=1}^{2}\left(4\nu^{2k-3}+3\right) \times\chi_k \sin\kappa_k \cos\left(\psi_p+\zeta_k\right) \ ,$$

$$\bar{\dot{\alpha}}^{SS} = -\frac{3\eta\pi}{\mathfrak{T}\,\bar{\mathfrak{l}}_r^4}\chi_1\chi_2 \times\left[\sin\kappa_1\cos\kappa_2\cos\left(\psi_p+\zeta_1\right) +\cos\kappa_1\sin\kappa_2\cos\left(\psi_p+\zeta_2\right)\right] \ ,$$

$$\bar{\dot{\alpha}}^{QM} = -\frac{3\eta\pi}{2\mathfrak{T}\,\bar{\mathfrak{l}}_r^4}\sum_{k=1}^{2}\nu^{2k-3}w_k\chi_k^2 \times\sin 2\kappa_k\cos\left(\psi_p+\zeta_k\right) \ .$$

$$\bar{\dot{\alpha}}^{2PN} = 0 \ .$$

Longitude of the ascending node:

$$\bar{\dot{\phi}}_n^{PN} = 0 \ ,$$

$$\bar{\dot{\phi}}_n^{SO} = -\frac{\eta\pi}{\mathfrak{T}\,\bar{\mathfrak{l}}_r^3\sin\alpha}\sum_{k=1}^{2}\left(4\nu^{2k-3}+3\right) \times\chi_k\sin\kappa_k\sin\left(\psi_p+\zeta_k\right) \ ,$$

$$\bar{\dot{\phi}}_n^{SS} = \frac{3\eta\pi}{\mathfrak{T}\,\bar{\mathfrak{l}}_r^4\sin\alpha}\chi_1\chi_2 \times\left[\sin\kappa_1\cos\kappa_2\sin\left(\psi_p+\zeta_1\right) +\cos\kappa_1\sin\kappa_2\sin\left(\psi_p+\zeta_2\right)\right] \ ,$$

$$\bar{\dot{\phi}}_n^{QM} = \frac{3\eta\pi}{2\mathfrak{T}\,\bar{\mathfrak{l}}_r^4\sin\alpha}\sum_{k=1}^{2}\nu^{2k-3}w_k\chi_k^2 \times\sin 2\kappa_k\sin\left(\psi_p+\zeta_k\right) \ ,$$

$$\bar{\dot{\phi}}_n^{2PN} = 0 \ .$$

Argument of the periastron:

$$\bar{\dot{\psi}}_p^{PN} = \frac{6\pi}{\mathfrak{T}\,\bar{\mathfrak{l}}_r^2} \ ,$$

$$\bar{\dot{\psi}}_p^{SO} = -\frac{\eta\pi}{\mathfrak{T}\,\bar{\mathfrak{l}}_r^3}\sum_{k=1}^{2}\left(4\nu^{2k-3}+3\right) \times\chi_k\left[2\cos\kappa_k +\cot\alpha\sin\kappa_k\sin\left(\psi_p+\zeta_k\right)\right] \ ,$$

$$\bar{\dot{\psi}}_p^{SS} = \frac{3\eta\pi}{\mathfrak{T}\,\bar{\mathfrak{l}}_r^4}\chi_1\chi_2 \times\left\{\cot\alpha\left[\sin\kappa_1\cos\kappa_2\sin\left(\psi_p+\zeta_1\right) +\cos\kappa_1\sin\kappa_2\sin\left(\psi_p+\zeta_2\right)\right]+2\cos\kappa_1 \times\cos\kappa_2-\sin\kappa_1\sin\kappa_2\cos\left(\zeta_2-\zeta_1\right)\right\} \ ,$$

$$\bar{\dot{\psi}}_p^{QM} = \frac{3\eta\pi}{2\mathfrak{T}\,\bar{\mathfrak{l}}_r^4}\sum_{k=1}^{2}\nu^{2k-3}w_k\chi_k^2 \times\left[\cot\alpha\sin 2\kappa_k\sin\left(\psi_p+\zeta_k\right) -3\sin^2\kappa_k+2\right] \ ,$$

$$\bar{\dot{\psi}}_p^{2PN} = \frac{3\pi}{2\mathfrak{T}\bar{\mathfrak{l}}_r^4}\left[33\bar{e}_r^2-4\eta-6\bar{e}_r^2\eta+2\right] \ .$$

→ The 2PN secular dynamics is simpler then the instantaneous dynamics

The 2PN secular dynamics: Spin angles

Spin polar angles:

$$\bar{\kappa}_i^{PN} = 0 \ ,$$

$$\begin{aligned}\bar{\kappa}_i^{SO} &= \frac{\eta\pi}{\mathfrak{T}\,\bar{\mathfrak{l}}_r^3} \\ &\times \left(4\nu^{2j-3}+3\right)\chi_j \sin\kappa_j \sin\left(\zeta_i-\zeta_j\right) \ ,\end{aligned}$$

$$\begin{aligned}\bar{\kappa}_i^{SS} &= -\frac{\eta\pi}{\mathfrak{T}\,\bar{\mathfrak{l}}_r^4}\chi_j \sin\kappa_j \\ &\times \sin\left(\zeta_i-\zeta_j\right)\left(2\bar{\mathfrak{l}}_r\nu^{2j-3}+3\chi_i\cos\kappa_i\right) \ ,\end{aligned}$$

$$\begin{aligned}\bar{\kappa}_i^{QM} &= -\frac{3\eta\pi}{2\mathfrak{T}\,\bar{\mathfrak{l}}_r^4}\nu^{2j-3}w_j\chi_j^2 \\ &\times \sin 2\kappa_j \sin\left(\zeta_i-\zeta_j\right) \ ,\end{aligned}$$

$$\bar{\kappa}_i^{2PN} = 0 \ ,$$

Spin azimuthal angles:

$$\bar{\zeta}_i^{PN} = -\bar{\psi}_p^{PN} \ ,$$

$$\begin{aligned}\bar{\zeta}_i^{SO} &= \frac{\eta\pi}{\mathfrak{T}\,\bar{\mathfrak{l}}_r^3}\left\{\bar{\mathfrak{l}}_r\left(4+3\nu^{3-2i}\right)\right. \\ &+3\left(4\nu^{2i-3}+3\right)\chi_i\cos\kappa_i+\left(4\nu^{2j-3}+3\right)\chi_j \\ &\times\left.\left[2\cos\kappa_j+\cot\kappa_i\sin\kappa_j\cos\left(\zeta_i-\zeta_j\right)\right]\right\}\end{aligned}$$

$$\begin{aligned}\bar{\zeta}_i^{SS} &= -\frac{2\eta\pi}{\mathfrak{T}\,\bar{\mathfrak{l}}_r^3}\nu^{2j-3}\chi_j\left[\cos\kappa_j\right. \\ &+\left.\cot\kappa_i\sin\kappa_j\cos\left(\zeta_i-\zeta_j\right)\right] \\ &-\frac{3\eta\pi}{\mathfrak{T}\,\bar{\mathfrak{l}}_r^4}\chi_i\chi_j \\ &\times\left\{\cot\kappa_i\left[3\sin\kappa_i\cos\kappa_j\right.\right. \\ &+\cos\kappa_i\sin\kappa_j\cos\left(\zeta_i-\zeta_j\right)] \\ &-\left.\left.\sin\kappa_i\sin\kappa_j\cos\left(\zeta_i-\zeta_j\right)\right\} \ ,\end{aligned}$$

$$\begin{aligned}\bar{\zeta}_i^{QM} &= -\frac{6\eta\pi}{\mathfrak{T}\,\bar{\mathfrak{l}}_r^3}w_i\chi_i\cos\kappa_i \\ &-\frac{3\eta\pi}{2\mathfrak{T}\,\bar{\mathfrak{l}}_r^4}\sum_{k=1}^{2}w_k\nu^{2k-3}\chi_k^2 \\ &\times\left[\left(2-3\sin^2\kappa_k\right)\right. \\ &+\left.\cot\kappa_i\sin\left(2\kappa_k\right)\cos\left(\zeta_i-\zeta_k\right)\right] \ ,\end{aligned}$$

$$\bar{\zeta}_i^{2PN} = -\bar{\psi}_p^{2PN} \ .$$

→ The 2PN secular dynamics is simpler then the instantaneous dynamics

The validity of the 2PN secular dynamics

Secular precessing compact binary dynamics, spin and orbital angular momentum flip-flops
M.Tápai, Z. Keresztes, L. Á. Gergely, LIGO Document P1600207, submitted to Phys. Rev D

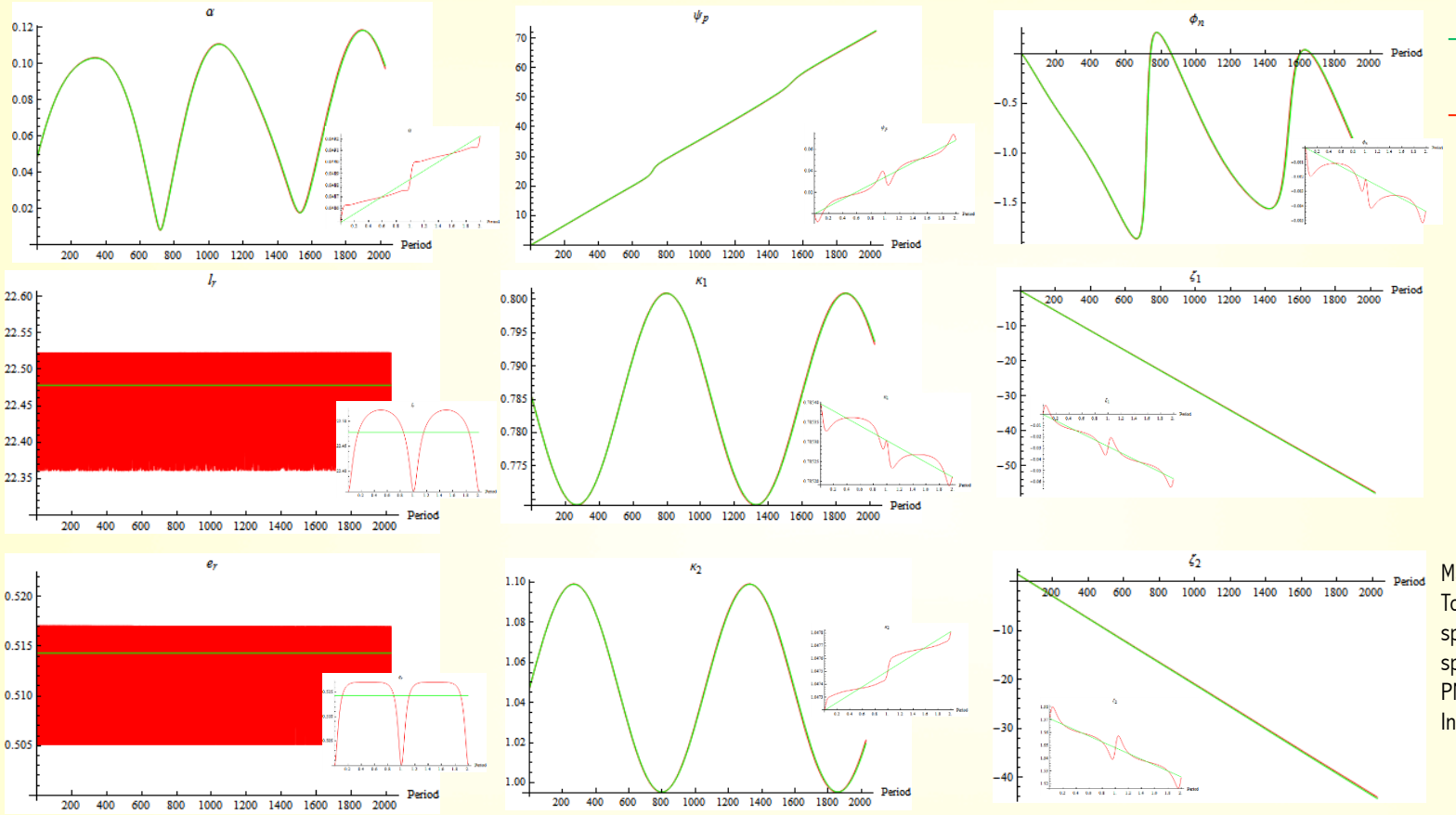

Mass ratio: 1:2
Total mass: 40 Solar masses
spin1 = 0.8
spin2 = 0.4
PN parameter = 0.003
Initial eccentricity = 0.5

3 time scales:

orbital period << precessional period << conservative time-scale (no significant change due to GWs)

230 orbital periods 2000 orbital periods
8 precessional periods

→ The 2PN secular dynamics can replace the instantaneous dynamics both on precessional and conservative time-scales

Application 2: Investigating the flip-flop effect

The smaller second spin ventures from one pole to the other – found numerically for particular configurations
C. O. Lousto, J. Healy, Flip-flopping binary black holes, Phys. Rev. Lett. **114**, 141101 (2015).

We are able to analyse the occurrence and significance of this effect analytically !

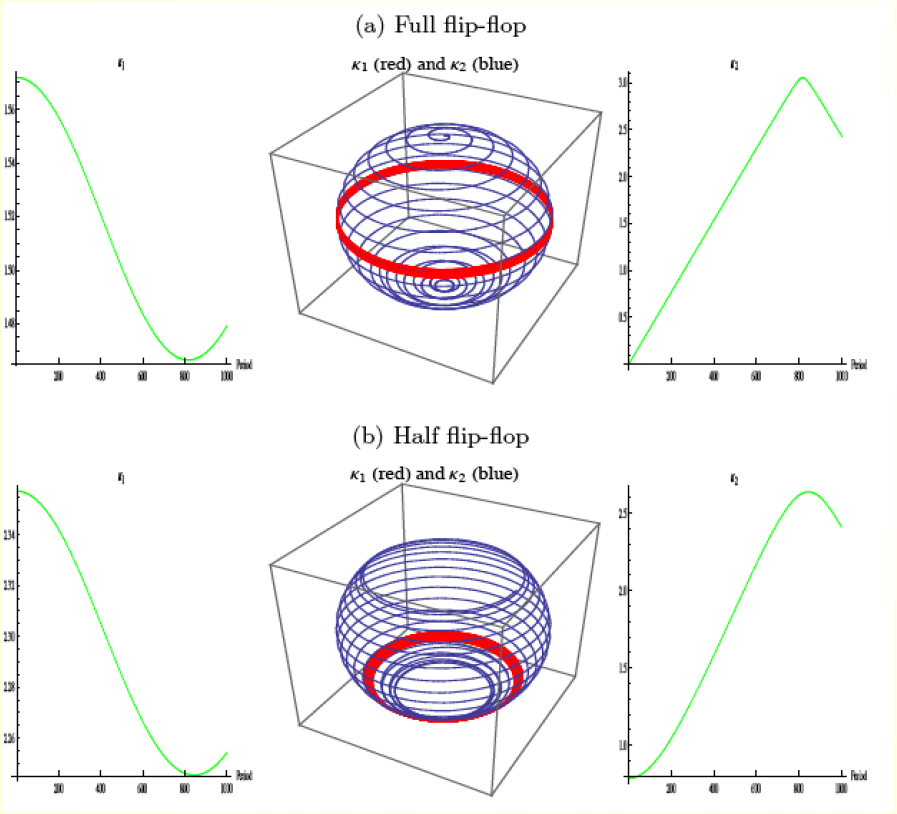

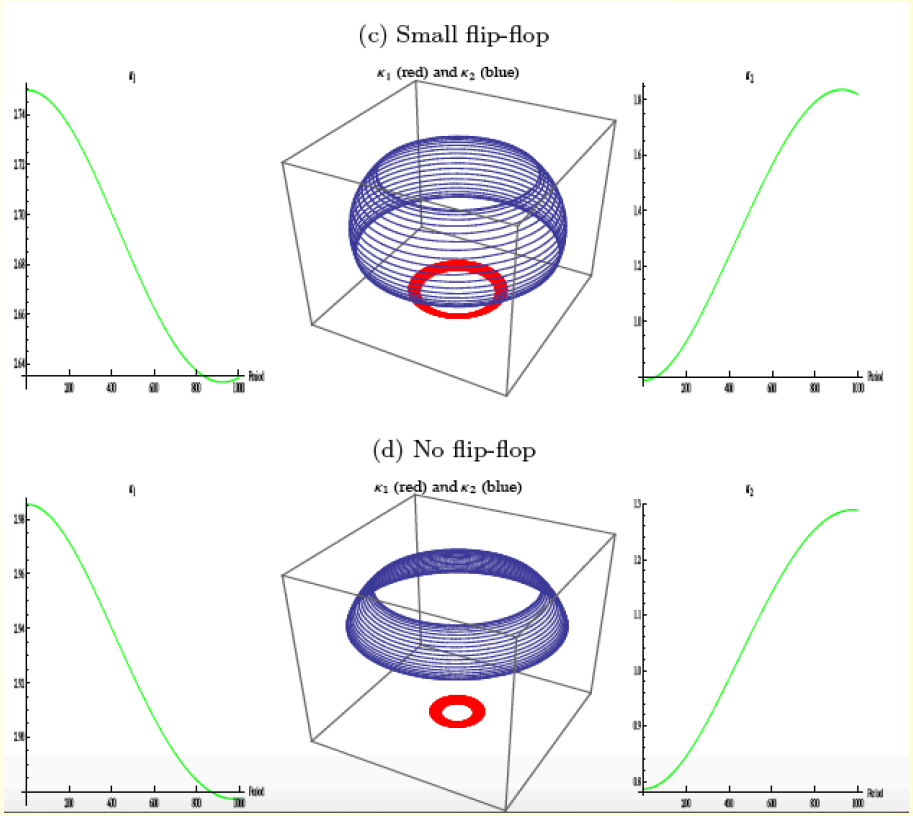

Secular precessing compact binary dynamics, spin and orbital angular momentum flip-flops
M.Tápai, Z. Keresztes, L. Á. Gergely, LIGO Document P1600207, submitted to Phys. Rev D

Application 2: Investigating the flip-flop effect

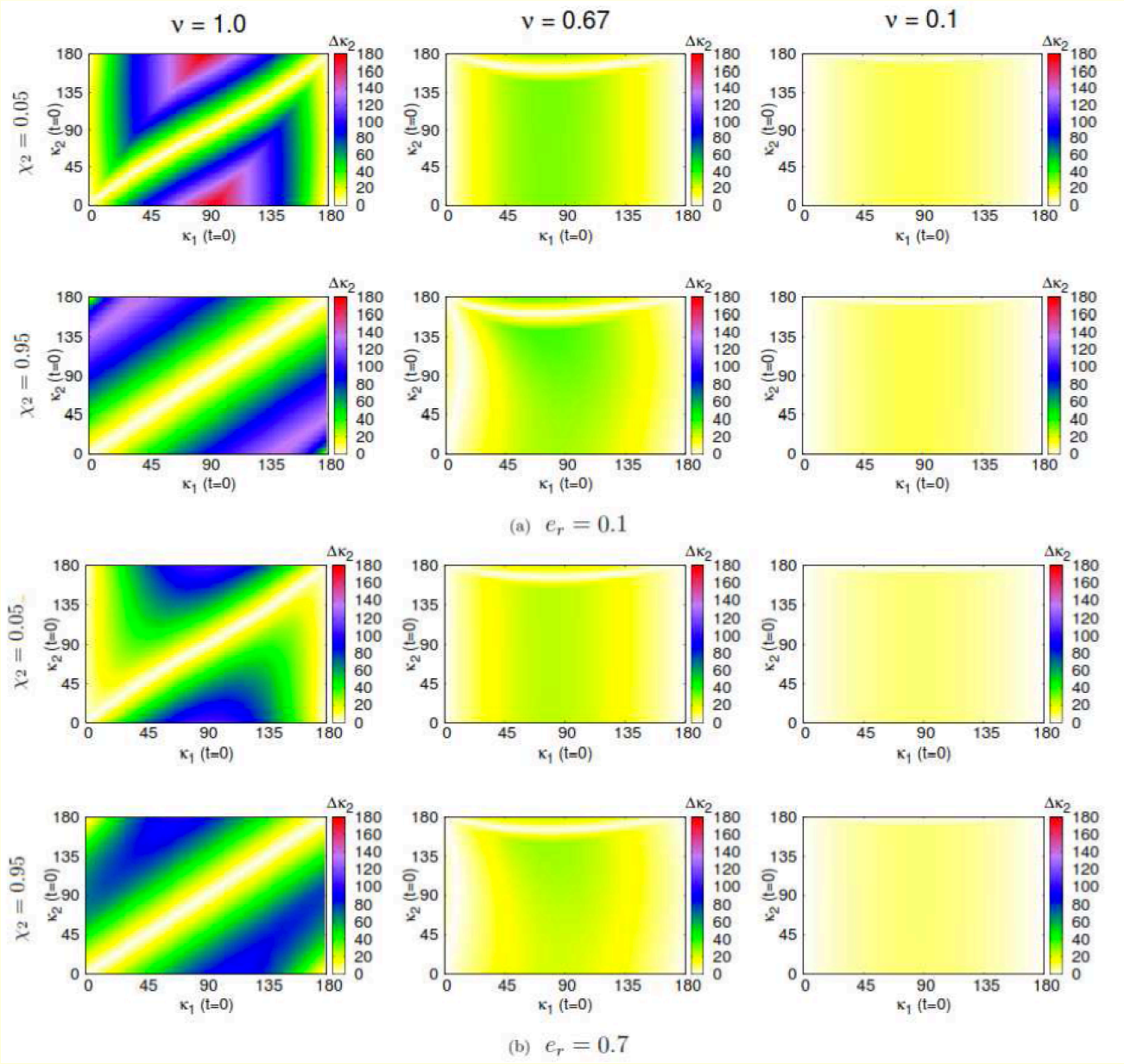

(a) $e_r = 0.1$

(b) $e_r = 0.7$

Gravitational wave affected time-scales: Our group participates in the Advanced LIGO data-analysis

Preliminary activity:

Márton Tápai (SZTE) and Mátyás Vasúth (Wigner)
visited the Observational Relativity and Cosmology Group of the Albert Einstein Institute in Hannover

Where they became accustomed with:

- The pycbc analysis scripts https://github.com/ligo-cbc/pycbc
- The pycbc search pipeline

Data analysis for Advanced LIGO:

In 2017 Márton Tápai actively participated in the pycbc data analysis

Was the lead pycbc analyst twice
(for 5 days of coincident data analysis chunks each)
for the O2 data collection

Application 3. The spin-flip effect

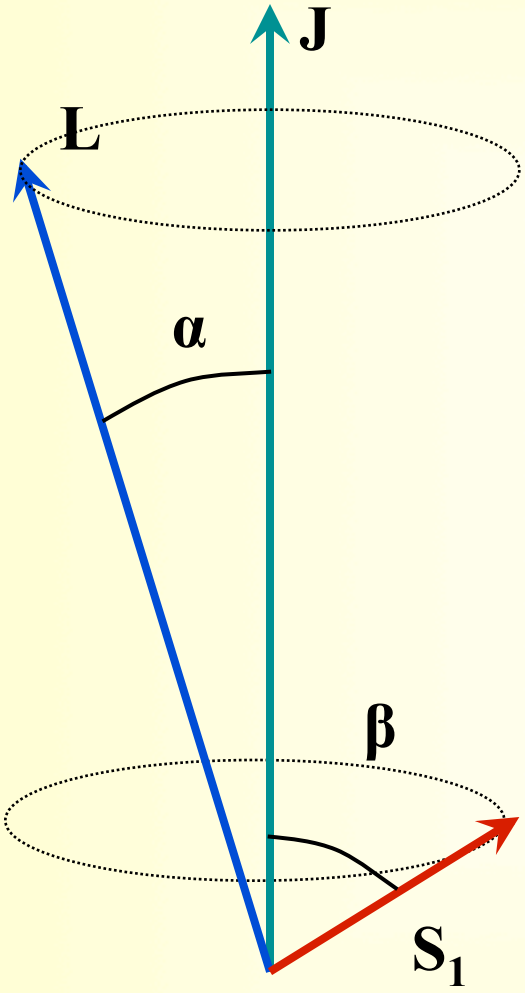

• due to GW emission the spin aligns to the original **J** direction

The spin-flip phenomenon in supermassive binary black hole mergers
L. Á. Gergely, P. L. Biermann,
Astrophys. J. **697,** 1621 (2009)

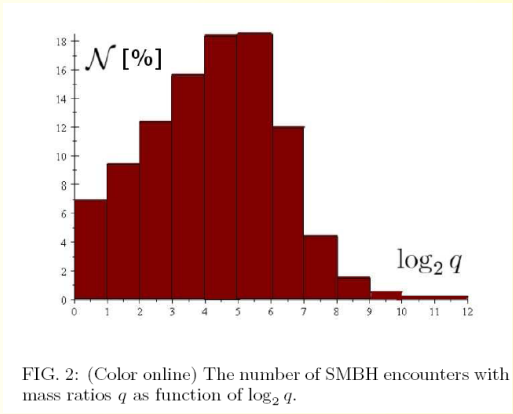

FIG. 2: (Color online) The number of SMBH encounters with mass ratios q as function of $\log_2 q$.

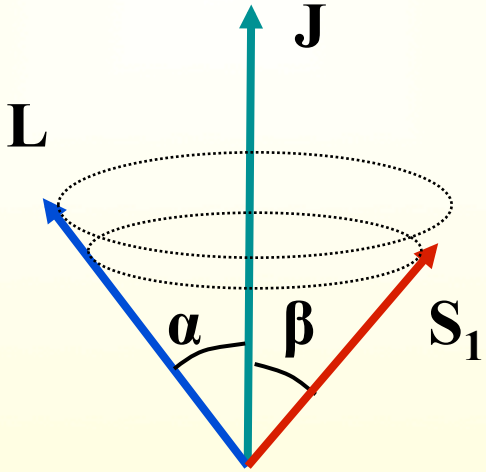

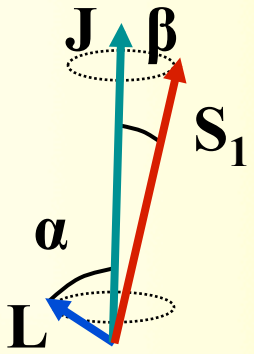

Key elements: (i) typically the BHs are not equal mass, $m_2 << m_1$, neglect $S_2 \sim m_2^2$

(ii) the direction of **J** is conserved, (iii) the magnitude of $\mathbf{S_1}$ is conserved → spin-flip

Application 3. The spin-flip effect: time-scales

Table 2: Order of magnitude estimates for the inspiral rate $\dot{L}/L$, angular precessional velocity Ω_p and tilt velocity $\dot{\alpha}$ of the vectors $\mathbf{L}$ and $\mathbf{S_1}$ with respect to $\mathbf{J}$, represented for the three regimes with $L > S_1$, $L \approx S_1$ and $L < S_1$, characteristic in the domain of mass ratios $\nu = 0.3 \div 0.03$. The numbers in brackets represent inverse time scales in seconds^{-1}, calculated for the typical mass ratio $\nu = 10^{-1}$, post-Newtonian parameter 10^{-3}, 10^{-2} and 10^{-1}, respectively and $m = 10^8 M_\odot$ (then $c^3/Gm = 2 \times 10^{-3}$ s^{-1}).

	$L > S_1$		$L \approx S_1$		$L < S_1$	
$-\dot{L}/L$	$\frac{32c^3}{5Gm}\varepsilon^4\eta$	$(\approx 10^{-15})$	$\frac{32c^3}{5Gm}\varepsilon^4\eta$	$(\approx 10^{-11})$	$\frac{32c^3}{5Gm}\varepsilon^4\eta$	$(\approx 10^{-7})$
Ω_p	$\frac{2c^3}{Gm}\varepsilon^{5/2}\eta$	$(\approx 10^{-11})$	$\frac{2c^3}{Gm}\varepsilon^{5/2}\eta\frac{J}{L}$	$\left(\approx 10^{-8}\frac{J}{L}\right)$	$\frac{2c^3}{Gm}\varepsilon^3$	$(\approx 10^{-5})$
$\frac{\dot{\alpha}}{\sin(\alpha+\beta)}$	$\frac{32c^3}{5Gm}\varepsilon^{9/2}\frac{\eta}{\nu}$	$(\approx 10^{-16})$	$\frac{32c^3}{5Gm}\varepsilon^{9/2}\frac{\eta}{\nu}\frac{L^2}{J^2}$	$\left(\approx 10^{-11}\frac{L^2}{J^2}\right)$	$\frac{32c^3}{5Gm}\varepsilon^{7/2}\eta\nu$	$(\approx 10^{-8})$

Time to merger:	30 million years	300 years	few months
Precession time scale:	3000 years	3 years	days
Variation of the tilt angle during one precession:	2 arcsec (6 x10^{-4} arcsec/year)		3 arcmin (/day)

Application 3. The spin-flip effect: magnitude

In the typical SMBH binaries the spin-flip occurs during the inspiral!

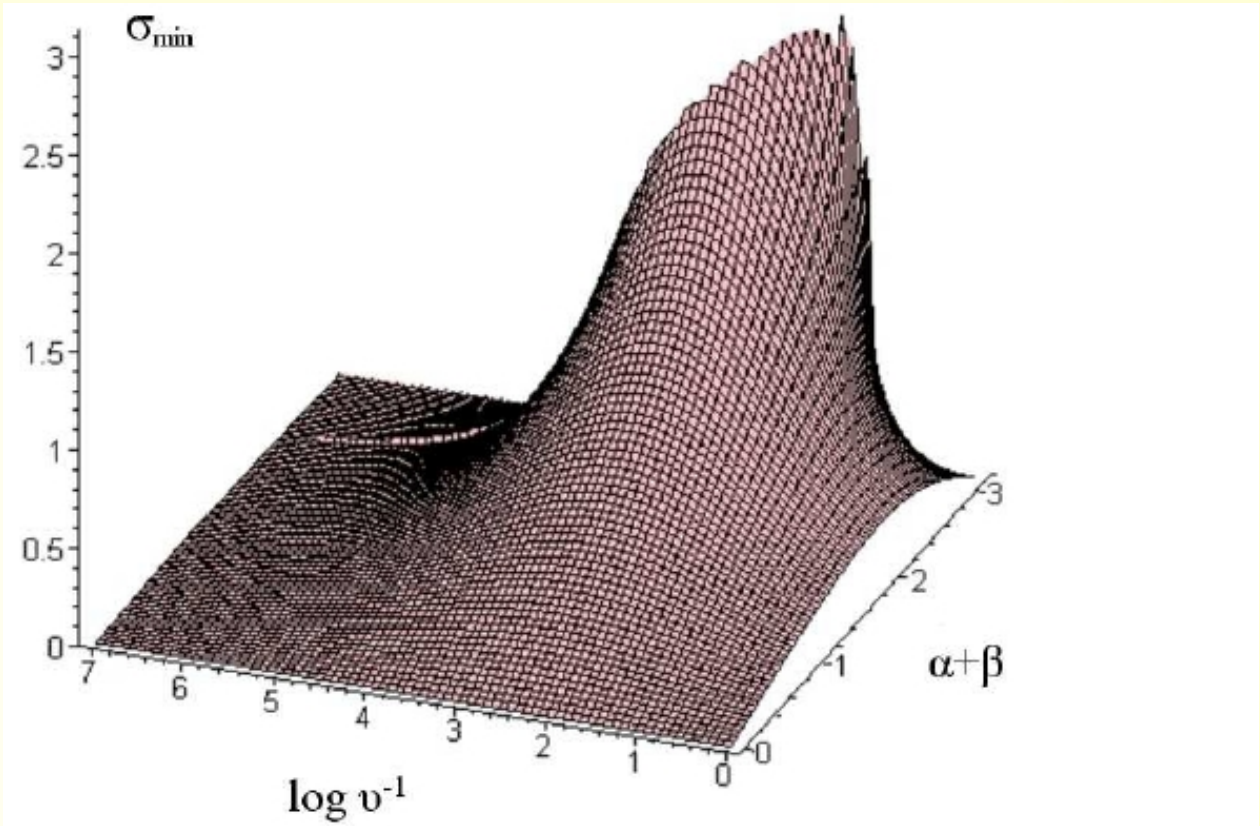

Figure 2. The spin-flip angle $\sigma_{\rm min}$ as function of the relative orientation of the spin and orbital angular momentum $\alpha + \beta$ (a constant during inspiral), and mass ratio ν. For a given mass ratio the spin-flip angle has a maximum shifted from $\pi/2$ towards the anti-aligned configurations. The mass ratios $\nu = 1;\ 1/3;\ 1/30$ and $1/1000$ are located on the $\log \nu^{-1}$ axis at 0; 1.09; 3.40 and 6.91, respectively, confirming the prediction, that a significant spin-flip will happen in the mass ratio range $\nu \in (1/30, 1/3)$. For mass ratios smaller than $1/100$ the spin does not flip at all, as the infalling SMBH acts as a test particle.

Supermassive black hole spin-flip during the inspiral
L. Á. Gergely, P. L. Biermann, L. I. Caramete, Class. Quantum Grav. **27** (2010) 194009

X-shaped radio galaxies: surviving witnesses of coalescing black hole binaries

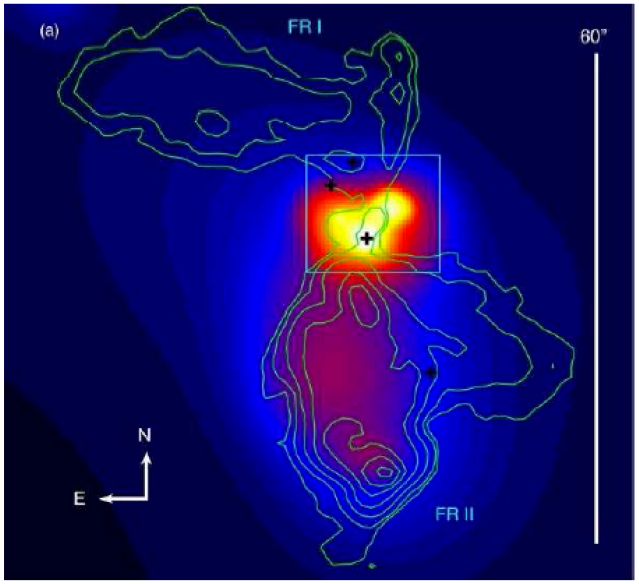

Fig. 1 Radio contours overlain on X-ray emission for the XRG 3C 433. Reprinted with permission from Miller & Brandt (2009); copyright AAS.

On the origin of X-shaped radio galaxies
Gopal-Krishna, P. L. Biermann, L. Á. Gergely, P. J. Wiita,
Research in Astron. Astrophys. **12**, 127–146 (**2012**)

Spin-flip model:	wing formation ceases before the primary lobes begin to form
Description	Jet direction flips due to re-alignment of the spin of the dominant SMBH, due to its merger with another SMBH.
Key merit/evidence	* Explains why hotspots are never seen in both lobe pairs. * Can explain secondary lobes being larger than primary lobes. * Post spin-flip, jets can easily propagate straight outwards. * Z-symmetry of the wings can be easily understood. * The empirically inferred systematic excess of SMBH mass in XRGs (compared to those in RGs) fits naturally into this picture. * Can also explain the formation of superdisks.
Does not naturally explain	* The correlation of the radio lobe axis with the optical axis of the host elliptical.

XRG catalog, post spin-flip radio galaxies

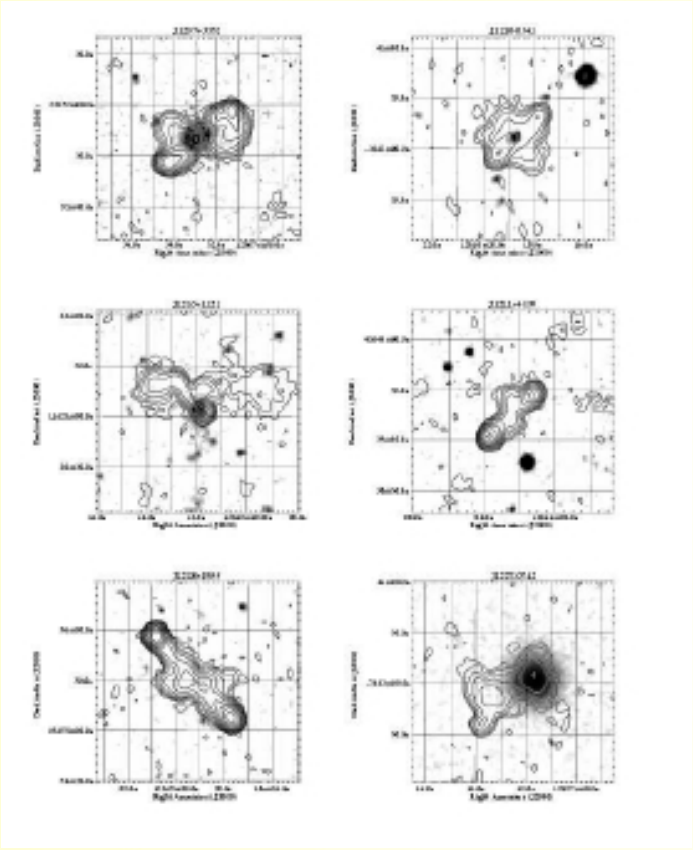

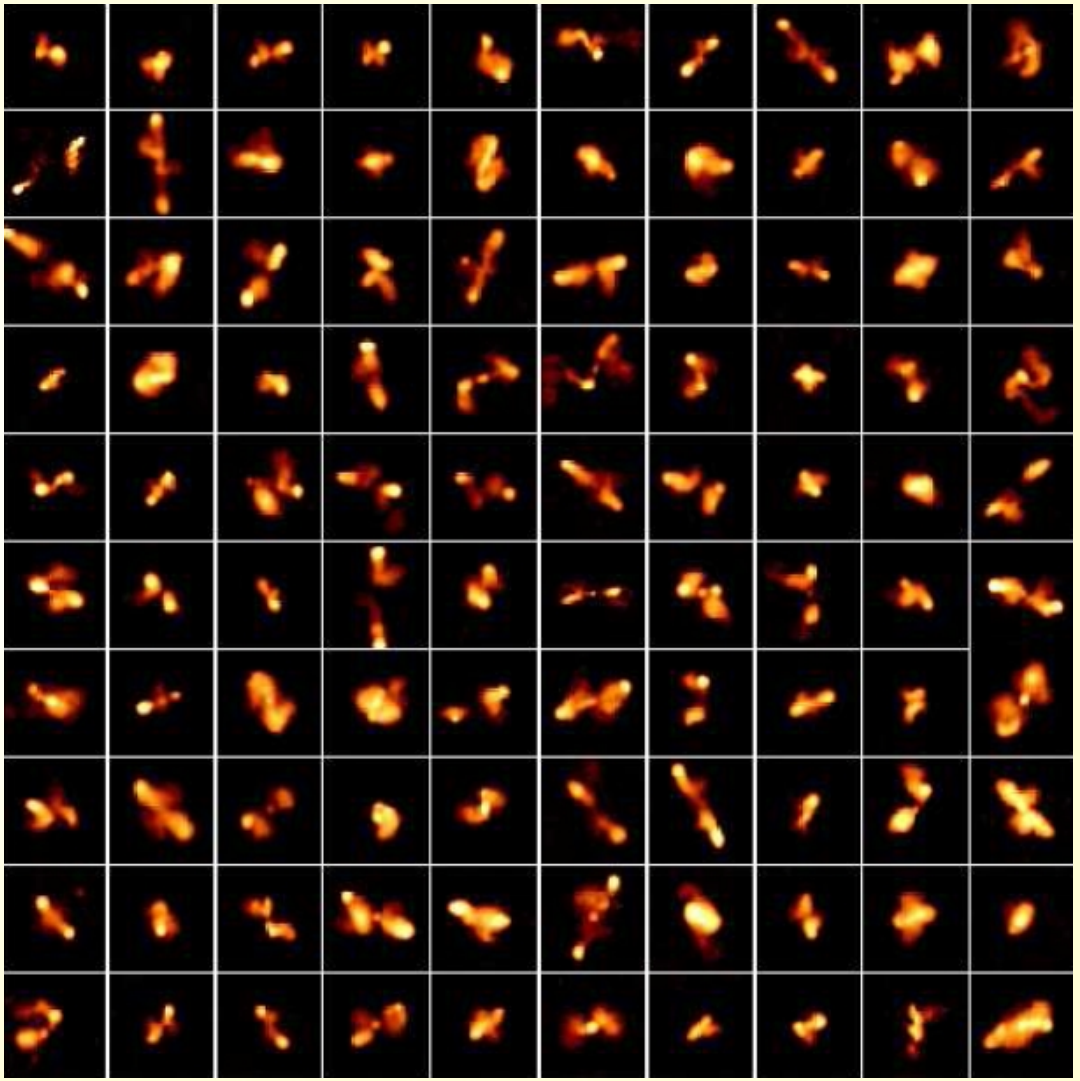

Cheung, C. C. :The Astronomical Journal, 133, 2097-2121 (2007), arXiv:astro-ph/0701278v3

The sky in supermassive black holes

Supermassive black hole spin-flip during the inspiral
L. Á. Gergely, P. L. Biermann, L. I. Caramete, Class. Quantum Grav. **27** (2010) 194009

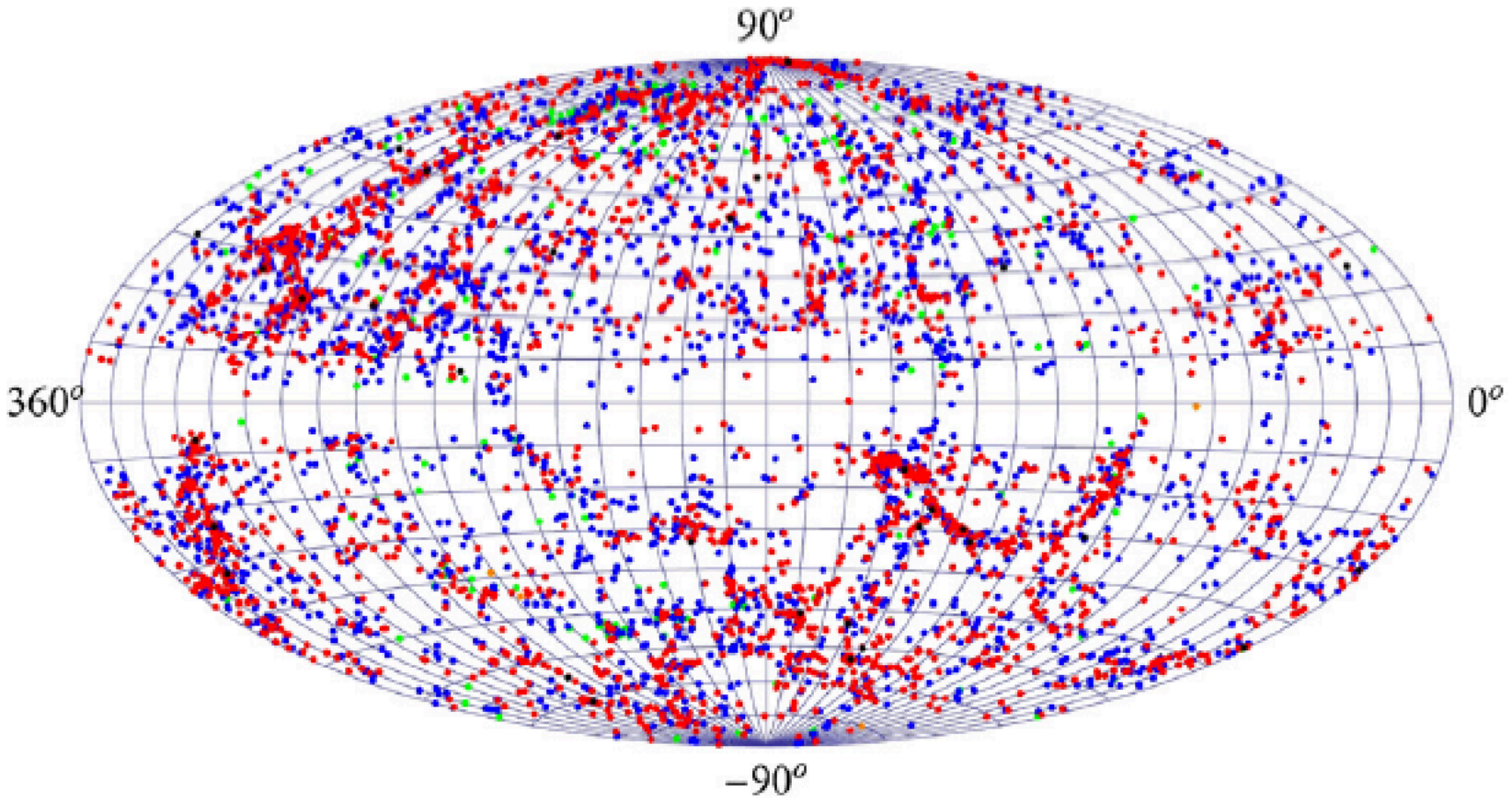

Figure 1. Aitoff projection in galactic coordinates of 5895 NED SMBH candidate sources. The sample is complete in a sensitivity sense; in order to derive densities one needs a volume correction. The color code (online only) is orange, green, blue, red, black corresponding to masses above $10^5\,M_\odot$, $10^6\,M_\odot$, $10^7\,M_\odot$, $10^8\,M_\odot$, $10^9\,M_\odot$, respectively. With the exception of the less numerous first range (orange), representing compact star clusters, the rest are SMBHs.

The sky in detected GWs (for now!!!)

Celestial sphere

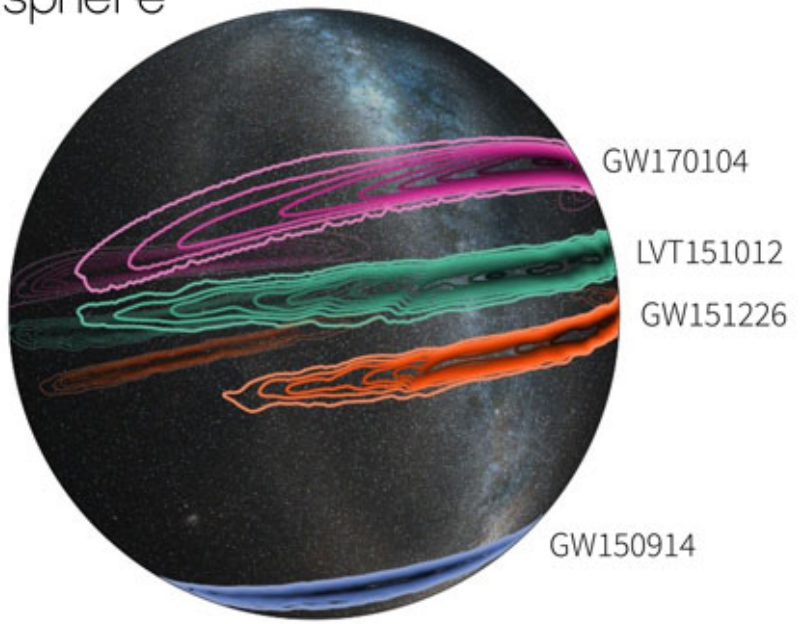

Aitoff projection

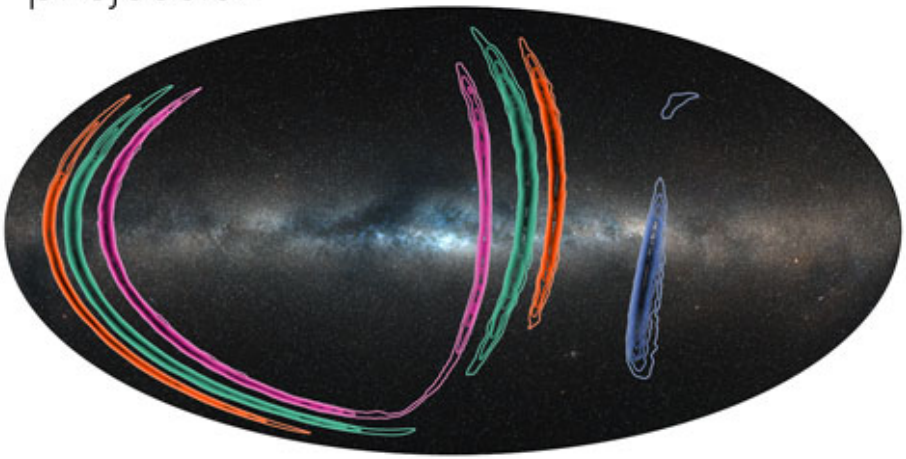

Localization will improve drastically with the new detectors

These are merely scratches on the GW sky!

Need new (and larger!) detectors (ET, DECIGO, LISA), in order to map the sky in GW at all frequencies !